Corrosion Science 168 (2020) 108586

Contents lists available at ScienceDirect

Corrosion Science

journal homepage: www.elsevier.com/locate/corsci

Corrosion investigation of fly ash based geopolymer mortar in natural sewer environment and sulphuric acid solution

Hammad A. Khan[a,*], Arnaud Castel[b], Mohammad S.H. Khan[c]

[a] NUST Institute of Civil Engineering, School of Civil and Environmental Engineering, National University of Sciences and Technology (NUST), Islamabad, 44000, Pakistan
[b] School of Civil and Environmental Engineering, University of Technology Sydney, NSW, 2007, Australia
[c] School of Engineering, Design and Construction, Melbourne Polytechnic, Melbourne, VIC 3076, Australia

ARTICLE INFO

Keywords:
Geopolymer
Microstructure
Acid solution
Microbiological corrosion
Corrosion models

ABSTRACT

The objective of this research is to estimate the durability of low-calcium fly ash based geopolymer mortar (FA-GPm) in comparison with sulphate resistant Portland cement mortars (SRPCm) exposed to natural sewer environment. Their performance is also investigated in the sulphuric acid (H_2SO_4) solution to highlight the difference in the corrosion mechanisms between these two exposure conditions. Mortar samples were removed from natural sewer and 1.5 % sulphuric acid solution after 12, 24 months and 6 months of exposure, respectively. Visual and physical analyses showed greater neutralization and loss in alkalinity in FA-GPm compared to SRPCm. However, mass loss and strength reduction observed for SRPCm was greater compared to FA-GPm. Microstructural analysis showed widespread gypsum crystallization within SRPCm matrix compared to FA-GPm, leading to more severe matrix deterioration. Differences in corrosion mechanism were identified between natural and sulphuric acid exposure conditions which led to the variation in estimated corrosion depth. Data collected from these microstructural and physical investigations were utilized to develop simplified linear models to express the depth of corrosion, surface pH, mass loss and neutralization depth of FA-GPm and SRPCm as a dependent of exposure time, temperature and H_2S concentration in natural sewer environments.

1. Introduction

Concrete is considered the fundamental material used for infrastructure development especially in sewage collection systems. This concrete experience rapid deterioration due to bacterial activity which not only impacts the environmental health but also cost millions of dollars for rehabilitation and to keep these structures running [1–3]. This biodegradation of concrete also known as 'microbial induced concrete corrosion' (MICC), impact the lifespan of concrete used for these infrastructure significantly by reducing it to around 30–50 years from the design life of 100 years (depending upon the aggressiveness of environment) [4].

MICC is a multistage complex microbiological and chemical process which initiates with the reduction of sulphate into hydrogen sulphide (H_2S) within the anaerobic zone of sewer by sulphur reducing bacteria [5,6]. Freshly casted concrete initially have the surface pH of around 12–13 (based on the type of concrete) [7–9]. Abiotic neutralization by carbonation and acidification of H_2S gas to thiosulphate and polythionic acid reduces this initial pH to around 9 particularly on the surface [10,11], making it suitable for the growth of sulphur oxidizing microorganisms (SOM). These chemical changes are followed by the initiation of the second stage of MICC. This phase initiate by the growth of microbiological colonies on the concrete surface. Initially, neutrophilic sulphur oxidizing microorganism (NSOM) grows on the surface of the concrete and produces sulphur based chemical (sulphur and poly-thionic acid) which causes the further reduction in the surface pH [12]. This initiates the corrosion of the concrete matrix. Main oxidation of H_2S to sulphate (SO_4^{2-}) usually have thiosulphate ($S_2O_3^{2-}$) and sulphur (S°) as intermediates, which acts as an energy source for many *Thiobacilli* SOM [13]. The most commonly available SOM which are involved in this microbiological corrosion include *Acidithiobacillus thiooxidans, Acidithiobacillus ferrooxidans, Thiomonas intermedia,* and *Halothiobacillus neapolitanus* [14,15]. Among these bacterial strains of SOM, *H. neapolitanus, T. intermedia* and *Acidithiobacillus thiooxidans* are the most aggressive strains which further deteriorates the concrete and were found within the pH ranges of 5.0–8.4 and 0.1–5.8, respectively [13,16]. Acidophilic SOM dominates the last stage by replacing these NSOM and cause additional reduction to the concrete pH especially on the surface to around 2.0 by metabolizing sulphur and thiosulphate into sulphuric acid (H_2SO_4) [1,17]. These stages of bacteriogenic corrosion

* Corresponding author.
E-mail address: hammad.anis@nice.nust.edu.pk (H.A. Khan).

https://doi.org/10.1016/j.corsci.2020.108586
Received 8 December 2019; Received in revised form 25 February 2020; Accepted 5 March 2020
Available online 07 March 2020
0010-938X/

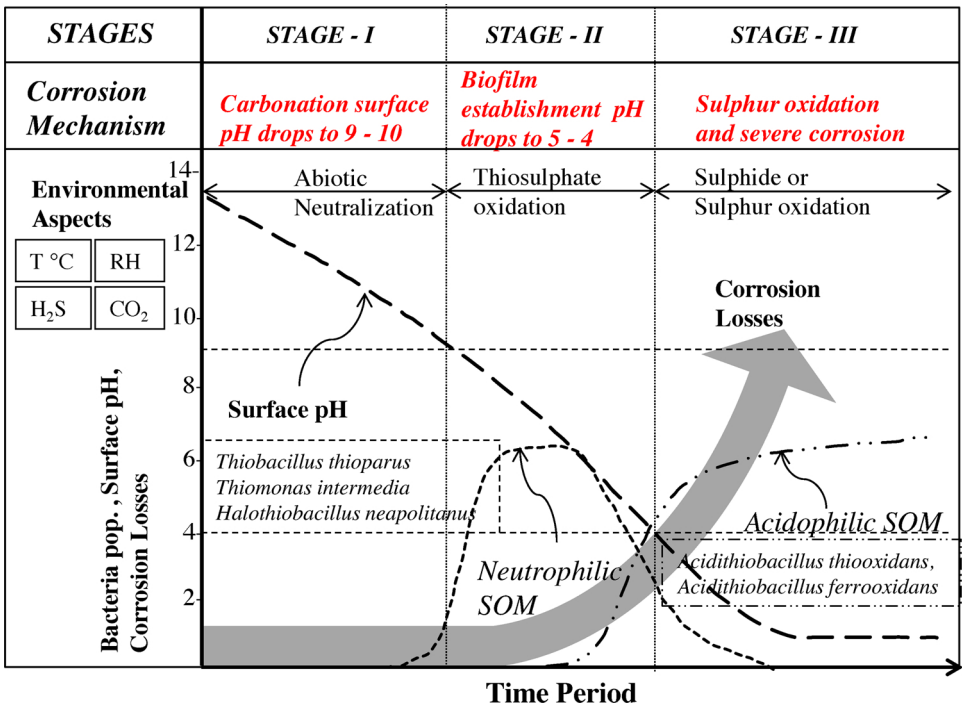

Fig. 1. Stages of MICC with hypothesized microorganism's succession and aspects causing deterioration in new concrete [10,17].

of concrete within aerobic zone were initially summarized and adopted by Islander et al. [10] (Fig. 1).

These bacterial activities under moist environment utilize sulphur and sulphates to form H_2SO_4 [18]. This leads to the disintegration and decalcification of cementitious phases within the matrix and causes the crystallization of sulphate salts within the exposed surface [2,19,20]. This biodeterioration not only effect the density of the concrete but also influence the physical and mechanical properties like porosity and strength [16,21]. These changes within the matrix lead to further penetration of acid and neutralization of deeper layers of concrete. Geopolymer concretes have potential to replace ordinary Portland cement (OPC) concrete for wastewater infrastructure development [22]. They are formed due to the reaction of secondary raw materials like metakoalin, fly ash (FA) and ground granulated blast-furnace slag (GGBS) with an alkaline activator made from metal hydroxide or silicate solution. During the alkali reaction with aluminosilicate-dominated FA binder, a network of highly cross-linked alkali-aluminosilicate was formed which is known as geopolymer [23,24]. This microstructure is build-up of randomly linked tetrahedrons of negatively charged $(SiO_4)^{-4}$ and $(AlO_4)^{-5}$ balanced by cation M^+ (Na^+ or K^+) in a three-dimensional network. This amorphous concrete which is being synthesized by using low-calcium fly ash and sodium silicate or hydroxide solutions as an alkaline activator forms sodium aluminosilicate (N-A-S-H) gel which is expected to perform well in an acidic environment [25,26]. Multiple researches were performed on these alkali activated GPCs against chemically induced corrosion by exposing them to H_2SO_4 [25,27–30]. The chemical resistance of geopolymer is dependent upon the dissociation of this amorphous gel matrix by liberation and replacement of proton (H^+) with alkali cation (Eq. (1)), followed by the breakage of the aluminosilicate network Si–O–Al and the removal of alumina [25]. This Al dissociation from the framework of aluminosilicate introduce vacancies for Si which join to form an imperfect silicic acid [25].

$$[Si - O - Al - O...]^- - M^+ + H^+ \rightarrow [Si - O - Al - O...]^- - H^+ + M^+ \quad (1)$$

Though, the performance of OPC based binder systems has been extensively investigated against microbially corrosive environment and sulphuric acid [1,2,4–6,10,16,20,31–34], the durability and performance of alkali-activated binders (fly ash and slag) in MICC environments needs to be assessed. Further, the cause of biodegradation from combined view point of material, chemical and microbial perspective needs to be evaluated for alkali-activated geopolymers which is important to improve the knowledge on biogenic corrosion and to prepare any counter active measures. Pilot research article compared the initiation phase of MICC (1st stage as per Fig. 1) within the matrix of fly ash (FA) geopolymer and alkali-activated ground granulated blast furnace slag (GGBFS) mortars exposed to the natural sewer environment exposed for the short term duration of one year [35]. However, geopolymer chemistry is time dependent and there is very little information available in the literature on this matter particularly in the context of biogenic corrosion where the development of SOB bacteria in governed by the long-term reduction in pore solution pH.

This paper investigates the advanced stages of MICC (Fig. 1) in fly ash geopolymer mortar (FA-GPm) specimens, having low calcium content, exposed to a natural sewer environment for a long term duration of two years. The performance of FA-GPm is compared to reference sulphate resistant Portland cement mortar (SRPCm). The same SRPCm was used as reference in another publication by the authors to assess and compare its durability with calcium aluminate cement based mortar [36]. In addition, deteriorations observed in natural sewage situation are compared to the effect of six months sulfuric acid attack aiming to assess the suitability of H_2SO_4 lab testing to simulate natural sewage conditions. Investigation techniques such as visual, physical and microstructural analysis were incorporated to establish the mechanism of corrosion. Moreover for the first-time, the data collected from 2 years field experimentation, empirical models are proposed to predict the deterioration of FA-GPm and SRPCm versus exposure time, temperature and H_2S concentration. To our knowledge, this is the first comparative study which analyses both long-term corrosion in natural sewer environment and sulphuric acid solution testing on low calcium FA-GPm by means of multiple physical, chemical and microstructural techniques.

Table 1
Mortar composition and compressive strength.

Components	FA-GPm (kg/m^3)	SRPCm (kg/m^3)
Fine Aggregate (silicon dioxide, SiO_2)	1230	1230
FA	522.75	–
GGBFS	92.25	–
Sulphate Resistant Portland cement (CEM-V)	–	615
12 M Sodium hydroxide solution (NaOH)	87.87	–
Sodium Silicate solution (Na_2SiO_3)	219.7	–
Free Water	25	258
Total Binder (SCM)	615	615
Water/binder*	0.31	0.42
Activator/SCM	0.5	–
Sodium Silicate/Sodium hydroxide (Na_2SiO_3/NaOH)	2.5	–
Modulus Ratio, Ms (SiO_2/Na_2O)	1.13	–
28 day Compressive Strength, (MPa)	46.3 ± 1.6	50.7 ± 1.7

Detailed batching and curing procedures are provided in [35] for FA-GPm and in [36] for SRPCm.

* Calculated by considering the total water (free water and the mass of water in the solutions) and total solids (SCM + anhydrous activator).

2. Experimental program

Two aluminosilicate sources namely, low-calcium fly ash (ASTM C 618 Class F) and Ground Granulated Blast Furnace Slag (GGBFS) were used to manufacture the geopolymer mortar (FA-GPm) [35]. Sulphate resistant Portland cement (SRPC) was used as a binder to manufacture sulphate resistant Portland cement mortar (SRPCm) [36]. The chemical composition and XRD patterns of fly ash and GGBFS are available in [35] and in [36] for SRPC cement. Sodium hydroxide (NaOH) solution and sodium silicate (Na_2SiO_3) solution mixture was used as activator for FA-GPm (see [35] for more details). Table 1 represents the mix proportioning of these mortars.

2.1. In field exposure

50 mm FA-GPm and SRPCm mortar cube specimens were placed in an approachable sewer chamber to analyse the deterioration after natural biogenic corrosion. North Head wastewater treatment plant (NHWTP) in Sydney was chosen for this field experimentation which runs for 24 h throughout 7 days. The mortar specimens were put in two different chambers connected with digesters. Specimens were hanged using stainless steel wires swaged with chemical resistant plastic net [35]. Proper monitoring of environmental conditions (temperature, humidity and H_2S concentration) was carried out using H_2S and temperature sensors at regular interval. The specimens were removed from chambers 1 and 2 for analysis after 6, 12 and 24 months of exposure. The deterioration of geopolymer after 6 and 12 months of infield exposure were described in a first publication by the authors [35]. This paper discusses the results obtained after 24 months of exposure.

2.1.1. Chambers atmospheric characterization

H_2S gas measurements data showed an average concentration over a period of two years to be around 53 and 27 ppm in chambers 1 and 2, respectively (Fig. 2) [36]. Relative humidity ranged from 78 % to 100 % (Fig. 2(a)). Maximum H_2S concentration observed was around 880 ppm and 706 ppm within chamber 1 and 2, respectively. Daily average H_2S gas concentrations in chamber 1 and 2 ranged between 0–195 ppm and 0–102 ppm respectively, depending upon the activeness of the digester and time of the day. The maximum observed daily average value for both chambers were adequate to sustain an aggressive environment, far above the minimum required concentration (10 ppm) to generate sulfuric acid [37]. Based on this assessment of H_2S gas concentration, chamber 1 environment was more corrosive compared to the second chamber. Moreover, by comparing the average of maximum H_2S gas per annum, it was estimated that, first chamber showed an increase in this concentration from 130 ppm in 12 months to 350 ppm after 2 year. On the other hand, this increase in H_2S concentration per annum was much reduced in chamber 2. This annual average was around 166 ppm in first year and after 2nd year it was observed to be around 232 ppm. This indicates that during the 1st year of exposure, both chambers were almost similar in severity; however during the 2nd year, the increase in annual H_2S gas concentration was greater in chamber 1. The average daily temperature assessed throughout 24 months of exposure inside the overflow chambers ranged between 34.1 and 13.7 °C, as shown in Fig. 2(b) [36]. The rise and fall of temperature inside the overflow chamber was due to the variation of outdoor atmospheric conditions and the temperature of the gas coming from the anaerobic digester. Grengg et al. measured the concentration of H_2S gas in combined sewer network having a maximum estimated concentration of 367 ppm, with an average of 6 ppm [2]. Wells and Melchers (2015) estimated the environmental conditions in two different sewers in Perth, Melbourne, and Sydney systems. The maximum H_2S gas concentration estimated was around 222 ppm, 5 ppm and 20 ppm within Perth, Melbourne and Sydney, respectively [38]. By comparing the severity of atmospheric conditions within the chamber 1 and 2 with these reported cases of manholes and sewer pipes, it was observed that the concentration of H_2S gas was higher in both chambers 1 and 2, confirming that the field conditions selected in this research was severe.

2.1.2. Testing after extraction of specimens

After the removal of specimens from infield environment, they were detached from the net assembly and were placed in the plastic bags. This procedure of removal from the natural sewer environment was adopted from Herisson et al. [34] and Kiliswa [39]. After the removal of organic slime from the surface, they were photographed to observe their visual variations and their surface pH was estimated. Water intrusion porosimetry was estimated following these initial physical observations to evaluate the bulk volume of permeable voids within the matrix. Mass and compressive strength were also measured to establish the variation in these physical properties after infield exposure. Moreover, depth of neutralization and profile of pH was also measured followed by the estimation of these physical parameters. In addition, microstructural studies, namely XRD, FTIR and SEM with EDX analysis were also performed on the FA-GPm and SRPCm specimens to observe the mineralogical formations and dissociation of matrix after exposure to an aggressive sewer environment. Section 2.3 provides the detailed description of each testing programme.

2.2. Sulphuric acid testing

50 mm FA-GPm and SRPCm mortar cube specimens were immersed in a 1.5 % of sulphuric acid solution (H_2SO_4). The concentration and pH of this acid solution were selected to be close to the acid concentration observed in the natural condition and represents the biodegradation of concrete in severe sewer conditions [18,40]. For more details about sulphuric acid attack, refer to [36].

2.3. Testing program

After the removal of mortar specimens from sulphuric acid and infield chamber, the following experimental procedures were adopted to evaluate the degradation and performance of mortars. Visual observations involved the evaluation of deterioration such as surface material removal, formation of surface cracks, and change in colour of the specimen using an optical light microscope. This microscope having the maximum magnification capability up to 100x was supported with Nikon DS-Ri1 camera for imaging. To estimate the variation in mass, specimens were oven dried for 24 h at 60 °C. The obtained mass was estimated and compared to the initial dry mass of the specimens before

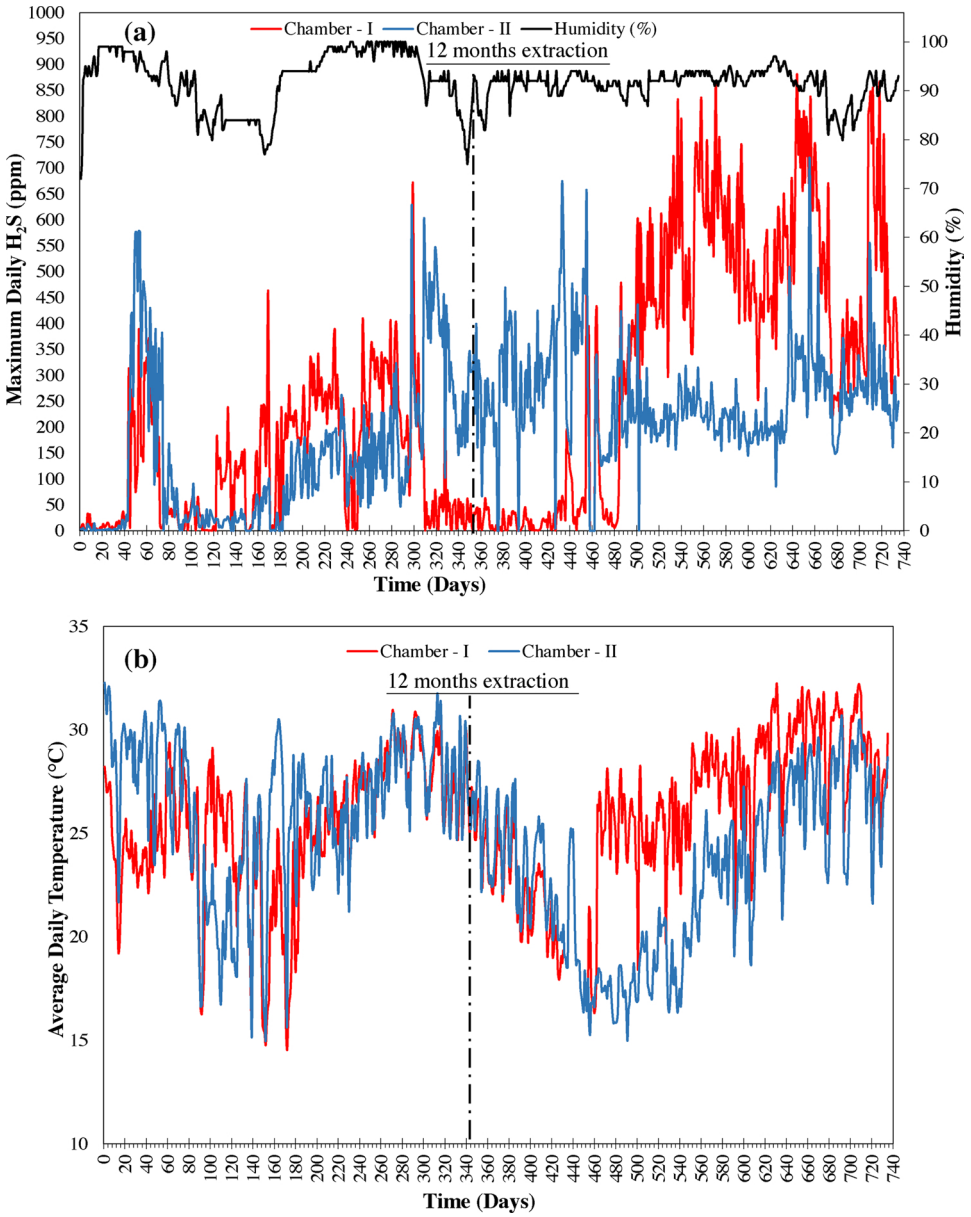

Fig. 2. Environmental conditions in chambers from the start of experiment: (a) maximum concentration of H_2S and averaged humidity, (b) Average daily temperature [36].

exposure to further validate the microstructural deterioration within these mortar specimen [41]. Bulk Volume of permeable voids were estimated according to ASTM C642-13 [42]. The FA-GPm and SRPCm specimens were kept in a vacuum condition for 4.5 h. Water was also vacuumed in the chamber to form de-aerated water which was pumped to another vacuum chamber having mortar specimens. These specimens were remained submerged underwater for 24 h after which the saturated mass (W_s) of these specimens were recorded. Apparent weight (W_a) of the specimen was also measured after saturation in vacuum chamber to estimate the volume of voids. After this, specimens were oven dried at 100 °C for 24 h to estimate the dry weight (W_d). The volume of permeable void was estimated using Eq. (2).

$$Volume\ of\ Permeable\ voids\ (VPV) = \frac{W_s - W_d}{W_s - W_a} \quad (2)$$

It is reported that after exposure to sewer environment the pH of concrete surface is reduced over time [43,44], which can be linked to the corrosion of concrete due to biogenic activities [10]. Hence, surface pH of specimens were assessed after 2 years of exposure using a pH probe having a flat face [45]. Deionized water was dropped on the surface of the specimen and 2 – 3 min was given to equilibrate, after which the pH of the droplet was estimated using the pH meter. The average surface pH was estimated by calculating 2 pH readings per each surface (except top and bottom sealed face). Failure load and compressive strength of specimens were evaluated as per ASTM C109 [46]. This compressive strength was estimated using the original cross-section before exposure to determine the loss in strength as suggested by Bassuoni, M. T. and Nehdi, M. L. [47]. To measure the alkalinity and depth of neutralization, phenolphthalein solution having concentration of 1% was sprayed on the split surface of the specimen [48–50]. The depth of neutralization observed was linked with the profile of pH to relate and validate the average neutralization depth of the mortar specimens. The pH profiles were estimated using the powder suspension method [51]. Thick slices of around 3 – 4 mm were cut from the specimen which was ground into powder. This powder was mixed with de-ionised distilled water for 5 min. The suspension had a solid to liquid ratio proportion of 1:1. Calibrated pH probe was used to estimate the pH of the suspension.

To analyse the formation of different mineralogical phases within the mortar matrix, microstructural investigations were performed. Powdered specimens at different depths from exposed surface were analysed using XRD and FTIR. Multipurpose diffractometer available at Mark Wainwright Analytical Centre at UNSW, Australia, was used to obtain the XRD patterns with a wavelength of 0.15418 nm from Cu–Kα radiation. These XRD patterns were obtained within the range of 5 – 70° and step size of 0·026° 2θ. Further analysis and phase identification was performed using the software package of X'pert High Score Plus. FTIR spectrums which identify the location of different phases of minerals within the microstructure of the mortar specimen were acquired using a Spotlight 400 FTIR spectrometer. 16 scans at 1 cm^{-1} resolution were attained within the range of 4000 to 650 cm^{-1} per sample. This microstructural investigation was done up to 15 mm depth after the exposure to natural sewer and acidic solution. The morphological changes within the microstructure of geopolymer and cement mortars were estimated using scanning electron microscope (SEM) with EDX analysis. For EDX analysis, the extracted SEM specimens were carbon coated to improve their conductivity and to enhance the imaging quality of microscopic images. The variation in the elemental concentration throughout the different matrices of FA-GPm and SRPCm after both infield and chemical acid exposure was analysed using the Hitachi S3400 electron microscope. The Electron Microscope equipment is available at the Mark Wainwright Analytical Centre of UNSW, Australia. The accelerating voltage was kept at 20 kV with a minimum working distance of 10 mm from the specimen. with the beam accelerating voltage of 20 kV. The overview of testing program for both exposure conditions is shown in Table 2.

3. Results and discussions

3.1. Visual and physical assessment with optical imagery

Both FA-GPm and SRPCm showed degraded surface after two years of exposure to natural sewer environment (Fig. 3). Smooth cubical surface with minor crack propagation near edges were observed by visual inspection of FA-GPm with no major efflorescence (Fig. 3(a–i)). SRPC mortars showed major degradation and loss of almost 2–3 mm material from the surface, as shown in Fig. 3(b–i). Further, a cross-section was also cut for both mixes, 10 mm from the top of the cube for the SEM analysis (location and dimension identified in Fig. 3a). Optical microscope imagery is performed on the SEM specimens obtained near the exposure surface. Signs of physical deterioration such as cracks, gaps and aggregate matrix debonding were observed in both mortars indicating the dissociation of the matrix. No major cracking within the whitish crystalline matrix of FA-GPm was observed even after 24 months of exposure. However, some permeable gaps were seen within the matrix which can be attributed to the breakage of the aluminosilicate matrix (Fig. 3(a-iii)) due to biogenic acid attack as discussed in Section 3.6. SRPCm showed noticeable matrix deterioration with the formation of cracks and gaps (Fig. 3(b-iii)), due to the formation of calcium sulphate salts [52]. However, no crystallization of salt or morphological changes within the hydrates can be seen at this magnification.

The optical microscope imagery was also done on both FA-GPm and SRPCm after six months of acid attack (Fig. 4). Minor surface disintegration on the edges of FA-GPm was observed, however, the bulk of geopolymer cube looked intact. In contrast, SRPCm specimen experienced major deterioration on the surface beside the formation of whitish sulphate salts on the surface (Fig. 4b-(i)). Further, optical microscope imagery of FA-GPm near exposure surface showed minor disintegration of matrix without the presence of any permeable void or cracks. Microscope imagery of SRPCm specimen showed three noticeable zones within the matrix; deteriorated; transition and intact (Fig. 4(b-iii)), as reported by Beddoe, R. E. and Dorner, H. W. [53], and identified by Berton et al. [54], and Bassouni, M. T. and Nehdi, M. L. [47]. Prominent change in colour can be seen within the three zones and can be attributed to the penetration and chemical reactions of sulphate ion from the acid solution with the matrix and the diffusion of alkali metals towards the solution [53]. The transition zone was identified having a yellowish colour and indicate the region up to which matrix is degraded and the ion exchange has taken place between acid solution and depth of disintegration of hydrates adjacent to undamaged core [53,55]. This zone is comprised of entirely aluminium, silicon, and iron after the disintegration of portlandite and C-S-H with in the matrix [54]. Corrosion depth and penetration of acid attack is dependent on the acid pH and the mineralogical composition of the mortar specimen. Moreover, this deterioration process also effects the microstructure by modifying the pore size distribution [53]. However, the precipitation of calcium sulphate reduces further sulphate anion diffusion flux towards the matrix. The $(OH)^{-1}$ released from the matrix reacts with H^{+} in the acid and neutralizes the pH of the solution. Hence, an increase in the

Table 2
Overview of testing program for infield and acid attack experiment.

Examination Parameters	Property tested	Testing Details	
		Infield exposure	Acid attack
Physical parameters	Visual inspection	Performed after 24 months	Performed after 6 months
	Surface pH (pH unit)	Estimated after 6, 12 and 24 months of infield exposure	–
	Loss in mass (%)	Same as above	Measured after 2, 4, 6, 8, 10, 12, 16, 20 and 24 weeks of acid exposure
	Failure Load (KN) and compressive Strength (MPa)	Tested after 24 months of exposure	Measured after 2, 4, 6, 8, 10, 12, 16, 20 and 24 weeks of acid attack
	Volume of Permeable voids (%)	Same as above	After 6 months in acid, the bulk porosity was measured
	Neutralization depth (mm)	Tested after 12 and 24 months of exposure	Tested after 4 and 6 months of acid exposure
	Profile of pH (pH unit)	Same as above	Same as above
acid solution testing	Leaching of elements using ICP (mg/L)	–	ICP analysis was performed after initial 7 and 14 days of testing, to estimate the leachates.
	pH of acid solution	–	pH of acid solution was periodically measured 4 times within every 14 days cycle
Microstructural analysis	XRD	Tested on the powdered sample extracted from corroded and un-corroded region after 24 months of exposure to infield conditions	Tested on the powdered sample extracted from corroded and un-corroded region after 6 months of acid exposure
	FTIR	Same as above	Same as above
	SEM with EDX	Tested on the polished and carbon coated samples extracted after 24 months of exposure to aggressive sewer environment	Tested on the polished and carbon coated samples extracted after 6 months of acid attack

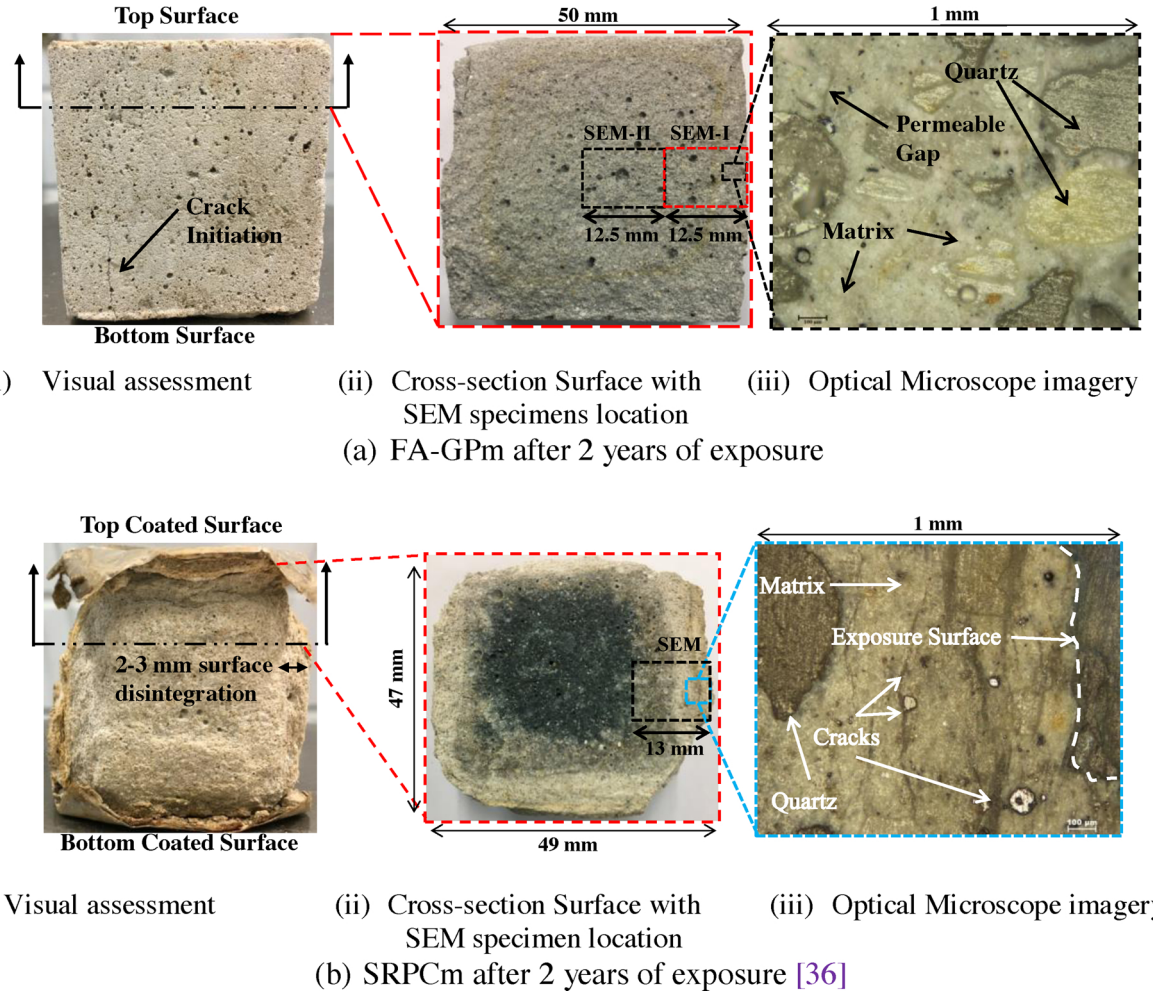

Fig. 3. Visual and Physical analysis of specimens using optical microscope imagery after 2 years of exposure in natural sewer environment.

neutralization indicate higher disintegration of binding matrix [56]. For FA-GPm, the deteriorated depth could not be identified, since there was no proper variation in colour. For SRPCm, an average transition zone was identified to be around 1.5 mm in addition to 2.5 mm of average deteriorated zone. This shows no restriction to diffusion of sulphate within the matrix of FA-GPm, indicating high ion exchange between matrix and acid solution. Further, phenolphthalein solution was also used to identify and validate the depth of deterioration for FA-GPm and SRPCm, respectively (Section 3.5).

3.2. Reduction in surface pH

Aggressiveness of the sewer environment on concrete can be highlighted in the form of loss in surface pH due to the growth of bacteria population followed by the loss in strength and deterioration of matrix [57]. Surface pH of SRPCm and FA-GPm estimated throughout this infield experimentation up to 12 months of exposure are adopted from previous publications by the authors [35,36]. 11.36 ± 0.1 and 12.6 ± 0.13 was the reference surface pH of FA-GPm and SRPCm, respectively, after 28 days of curing before the exposure to aggressive conditions. The loss in surface pH in both chambers is shown with respect to exposure time in Fig. 5. It is observed, that during first 6 months both mixes experience a major reduction in surface pH, followed by a steadier reduction till 12 months of exposure. In FA-GPm, the reduction in surface pH from chamber 1 and 2 environmental conditions was almost equivalent with an estimated average drop of around 3.4 and 3.22 over a period of 12 months, respectively. However for SRPCm, this pH reduction was much greater after 12 months of exposure, with an average drop of 4.35 and 3.77 in chamber 1 and 2, respectively. For FA-GPm, the change rate during initial 6 months was measured to be – 0.48 ± 0.02 pH units per month for both chambers, however, this pH drop was slowed down to around – 0.08 ± 0.02 pH units per month during next 6 months period. However, the rate of surface pH drop in SRPCm from chamber 1 during the initial 6 months was much higher with an average reduction of – 0.58 ± 0.04 pH units per month, followed by a steadier reduction rate of – 0.14 ± 0.03 pH units per month in the next 6 months period. This accelerated drop in surface pH during initial 6 months for both mixes can be linked to stage-I of abiotic neutralization caused by the concurrent carbonation and H_2S acidification.

Stage II of biotic growth and chemical corrosion initiates when the surface pH of specimen is reduced to pH below 9.0 (Fig. 1) [10]. Hence, the initiation of stage II is marked at a surface pH of 8.5 and is used to estimate the commencement of this stage with reference to exposure time (Fig. 5). It can be seen that FA-GPm specimens reached this transition from stage I to II at 6 months. In comparison SRPCm reached this transition after additional 4 and 8 months of exposure in chamber 1 and 2, respectively (Fig. 5). In previous studies, Robert et al. observed that this transition was achieved in 60–90 days when H2S concentration was 50 ppm [14], whereas, it was estimated by Okabe et al. [18] that this transition was achieved in just 56 days at 30 ± 20 ppm, indicating that stage I has a shorter duration and depends upon the exposure condition and concentration of H_2S. Since, the initial surface pH of SRPCm was more compared to FA-GPm, the shift from stage I to II of

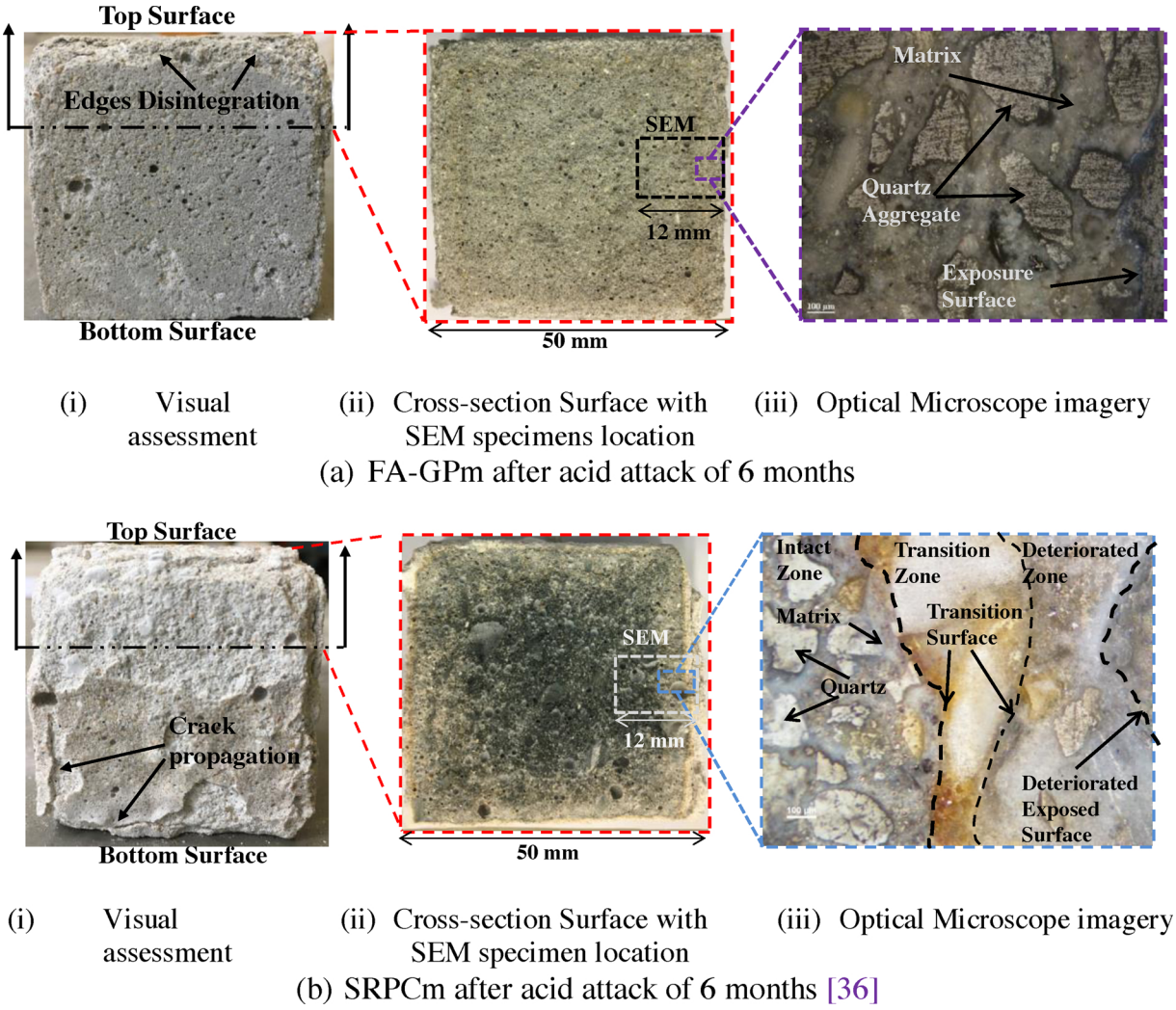

Fig. 4. Visual analysis and optical microscopy of specimens after exposure to sulphuric acid solution for 6 months.

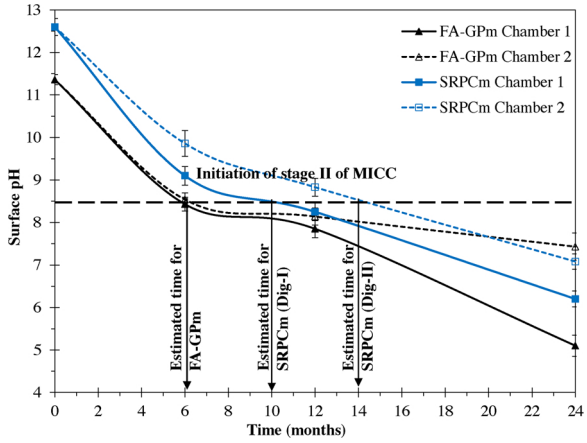

Fig. 5. Loss in surface pH after exposure to infield sewer environment.

MICC which requires a surface pH less than 9.0 was reached more quickly in FA-GPm.

The environmental conditions (H_2S concentration and temperature) recorded within the drain of chamber 1 showed a rise in annual average concentration of H_2S by more than 250 % within 12–24 months of exposure. Whereas in chamber 2, this rise in annual average H_2S concentration after 12 months of exposure was only 40 %, making it less aggressive in comparison to chamber 1 (Fig. 2). After one year of exposure, a steadier trend in drop of surface pH was observed for specimens collected from chamber 2 which can be linked to the much reduced rise in H_2S concentration. Further in chamber 2, the drop in surface pH of around 0.71 pH unit per annum was measured in FA-GPm. In comparison, higher reduction of 1.75 pH unit per annum was observed in SRPCm in this less aggressive chamber 2. This led to a much lower surface pH value in SRPCm as compared to FA-GPm (Fig. 5). In case of chamber 1, a much steeper drop with the loss of more than 2.0 pH unit was observed within 12–24 months of exposure for both types of mortars. Since the aggressiveness of the sewer environment is significantly affected by the variation in concentration of H_2S [37], the loss in surface pH was also significantly affected by this variation of H_2S concentration, irrespective of the type of mix.

3.3. Variation in mass, porosity and strength

Physical parameters and reduction in failure load were measured for both FA-GPm and SRPCm after 2 years exposure to the natural sewer environment and are summarized in Table 3 with reference to control specimens. Since the H_2S concentration in chamber 1 was much higher as compared to chamber 2, the overall physical degradation of these FA-GPm and SRPCm specimens in chamber 1 was much higher. It can be seen that the volume of permeable voids (VPV) of control FA-GPm and SRPCm specimens were similar. After exposure to infield deterioration both specimens experienced an increase in porosity. The FA-

Table 3
Porosity, Failure load, Compressive strength and Loss in mass of FA-GPm and SRPCm after 24 months exposure to natural sewer environment.

Physical Property	FA-GPm			SRPCm		
	Control	Chamber 1	Chamber 2	Control	Chamber 1	Chamber 2
Porosity (%)	18.4 ± 0.38	27.9 ± 0.07	22.5 ± 1.4	17.8 ± 0.1	23.4 ± 1.0	20.6 ± 0.31
Failure Load (KN)	130 ± 3	56.7 ± 7.4	111 ± 3.8	127 ± 3	33.7 ± 3.1	73 ± 7.5
Compressive Strength (MPa)	50.5 ± 0.97	22.3 ± 2.4	42.9 ± 1.9	49.3 ± 0.36	15.9 ± 2.3	27.9 ± 2.9
Mass Loss (%)	–	−7.4 ± 2.1	−3.5 ± 0.6	–	−19.2 ± 2.9	−7.5 ± 0.3

GPm specimens from both chambers showed greater rise in porosity as compared to SRPCm. This increase in VPV for FA-GPm ranged from 22.4% to 52% with respect to control specimen, whereas, this rise was only 15.5%–31.8% in SRPCm in chamber 2 and 1, respectively. However, it is observed that the loss in mass and compressive strength was much higher in SRPCm as compared to FA-GPm. Significant mass loss of around 7.5%–19.2% was observed in SRPCm due to surface spalling and crack propagation between aggregate and matrix, whereas in FA-GPm this mass loss ranged from 3.5% to 7.4% in chamber 2 and 1, respectively. In addition, SRPCm experienced a compressive strength loss of 43.3%–67.6% with respect to control specimen in chamber 2 and 1, respectively. For FA-GPm, this reduction in strength was only 15%–56% in chamber 2 and 1, respectively, confirming that the degradation in SRPCm was much more prominent compared to FA-GPm.

FA-GPm experienced a bulk increase in permeability and porosity with minor cracking and loss of surface material, whereas SRPCm experienced major cracking and loss of material from exposure surface due to precipitation of sulphates products (Fig. 3). This deterioration of SRPCm matrix is due to the formation of secondary phases such as gypsum and ettringite from primary hydrates (Portlandite and C-S-H) as a result of sulphate penetration, as shown in Eqs. (3)–(5) [19,58]. Gypsum crystallization alone leads to a volumetric expansion of 2.2 which leads to cracking of the matrix [6,47,59]. Further and in contrast with FA-GPm, nucleation of these secondary expansive phases within the permeable voids of degraded SRPCm matrix contributes to limit the rise in porosity.

$$Ca(OH)_2 + SO_4^{2-} + 2H_2O \rightarrow CaSO_4.2H_2O \quad (3)$$

$$xCaO.\ ySiO_2.\ zH_2O + SO_4^{2-} + 2H_2O \rightarrow CaSO_4.2H_2O + Si(OH)_4 \quad (4)$$

$$3CaO.\ Al_2O_3.\ CaSO_4.12H_2O + 2CaSO_4.2H_2O + 16H_2O \rightarrow 3CaO.\ Al_2O_3.3CaSO_4.32H_2O \quad (5)$$

To assess the performance of FA-GPm and SRPCm against sulphuric acid, variation in mass and strength were measured periodically and are shown in Fig. 6. These performance parameters were presented as a percentage of initial mass and strength measured before exposure. It is observed that SRPCm specimens, showed gain in mass of 1.4 % initially during the first 2 weeks, which was followed by a continuous loss in mass to around 14.3 % after six months of acid attack. This initial mass gain can be linked to the absorption of water and acid solution [28]. Reaction-diffusion phenomenon which was initiated after the exposure of specimen to acid solution, created internal micro-cracking after the formation of sulphate minerals from the reactions between cement hydrates and sulphuric acid [47]. After six months of exposure, the compressive strength reduction in SRPCm was much greater compared to mass loss (Fig. 6(b)), with an overall loss of 45.7 %.

The low-calcium fly ash based geopolymer specimens showed much better performance as compared to SRPCm specimens with only 4.8 % reduction in mass which was around 3 times less than OPC based mix. In addition, the loss in strength observed after 6 months of exposure was only 25 % of initial strength. Moreover, an accelerating trend in loss of mass and strength was observed in SRPCm, whereas a more stabilized decelerating trend was seen in FA-GPm suggesting better long-term durability of geopolymer in an acidic environment as compared to Portland cement mortar. The porosity of FA-GPm and SRPCm after exposure to sulphuric acid attack with reference to initial porosity before exposure is shown in Table 4. FA-GPm and SRPCm experienced an increase in porosity of 14.4 % and 10.1 %, respectively. This suggests that, similar to infield exposure, dissolution of geopolymer matrix due to acid attacks leads to the formation of permeable pores without major deterioration of the surface of the specimen. Further, the reduction in mass and strength of FA-GPm can be linked to this increase in bulk porosity. The geopolymer specimens looked intact with no major loss of surface material, unlike SRPCm due to crack propagation and disintegration of C-S-H matrix. The matrix of geopolymer seems more resilient to acid exposure. Bakharev [25], Lee, and Lee [29] and Aiken et al. [60] attributed the better performance of FA-GPm against acid attack to the higher durability of cross-linked sodium aluminosilicate (N-A-S-H) matrix. The better performance of FA-GPm can also be linked to differences in microstructure and degradation mechanics (see Sections 3.6 and 3.7).

3.4. pH Profile with respect to neutralization depth

Alkalinity of concrete is seriously affected after exposure to acidic environments. This leads to the deterioration of the matrix and, in case of reinforced concrete, can lead to corrosion of reinforcement [61]. This loss in alkalinity as the neutralization depth was estimated on the freshly fractured SRPCm and FA-GPm mortar surface by spraying 1%

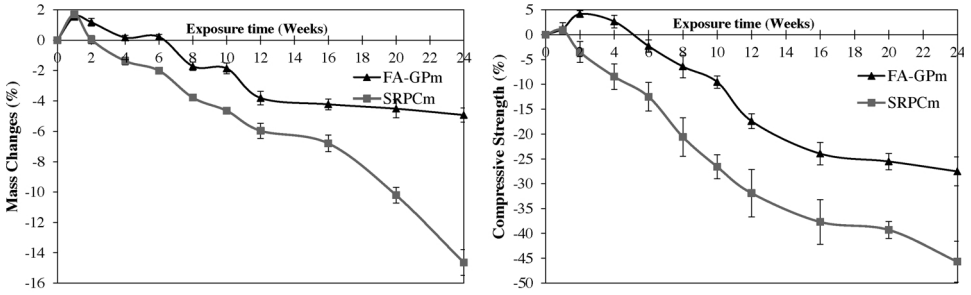

(a) Change in Mass (b) Change in compressive strength

Fig. 6. Percentage change in mass and strength of FA-GPm and SRPCm after acid exposure.

Table 4
Porosity of FA-GPm and SRPCm after six months of acid attack.

Type of specimen	Volume of Permeable void (%)	
	Before immersion	After immersion
FA-GPm	18.4 ± 0.1	21.0 ± 0.02
SRPCm	17.8 ± 0.11	19.6 ± 0.4

phenolphthalein solution, after exposure to an aggressive sewer environment for a time duration of 12 and 24 months and sulphuric acid solution for 4 and 6 months. This represents the depth up to which the diffusion of acid and loss in alkalinity has taken place beside the disintegration of matrix within the different types of mortars [49,60]. Reference pH profile of FA-GPm and SRPCm was also evaluated within the core having a pH of around 11.8 and 12.78, respectively. This core region having high alkalinity showed a dark pink colour with the application of phenolphthalein indicator [62].

The minimum pH of fully neutralized colourless region in carbonated fly ash geopolymer concrete was estimated to be around 10 [62]. Fig. 7 represents the depth of neutralization with respect to exposure time for FA-GPm. This neutralization depth was estimated by accounting for the original dimensions of the specimens before exposure. Complete neutralization of depth equal to 25 mm was observed for FA-GPm specimens from both chambers after one year of exposure. This is consistent with the pH less than 10.0 observed throughout 25 mm depth of specimen (Fig. 7(b)). Importantly, the estimated pH after 2 years of exposure was less than 9.0, with a lowest pH value of around 6.9 in chamber 1, depicting that MICC stage-II has been initiated within the microstructure of FA-GPm, after abiotic neutralization. The average depth of neutralization observed using phenolphthalein indicator is denoted as D (month of exposure)_(aggressive environment) and is

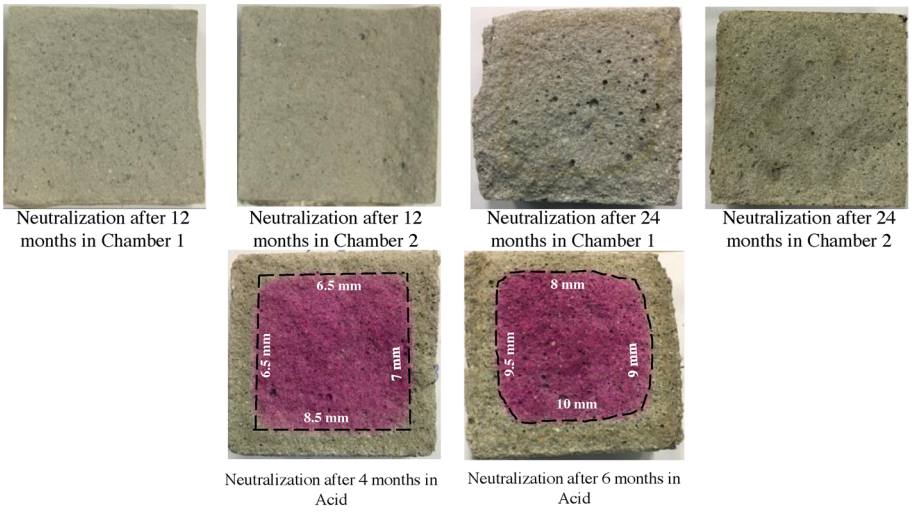

(a) Neutralization depths of FA-GPm

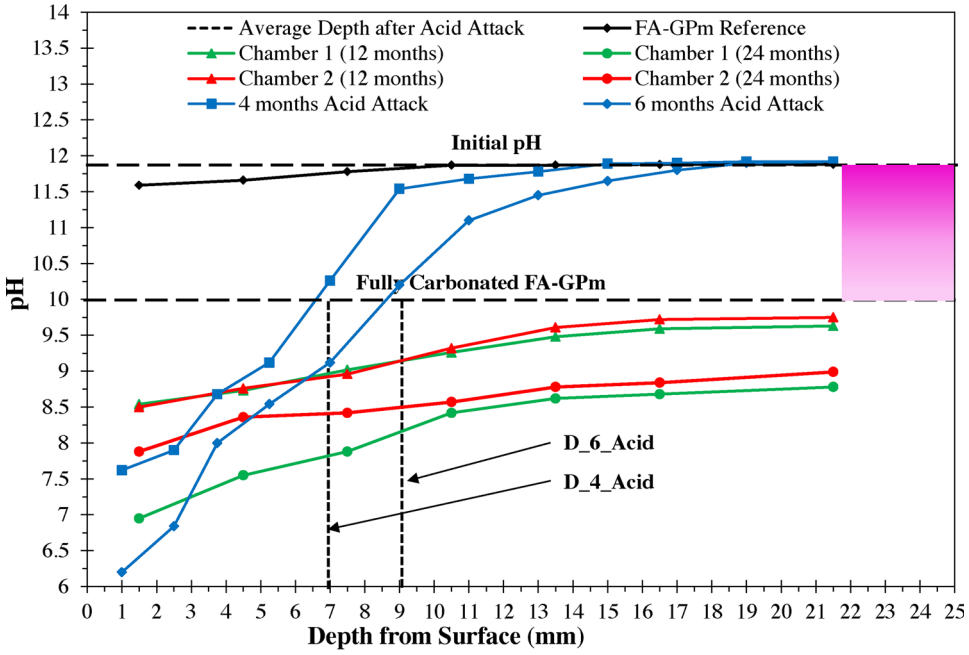

(b) FA-GPm pH profile

Fig. 7. Depth of neutralization and profile of pH of FA-GPm after infield sewer environments and sulphuric acid solution exposure.

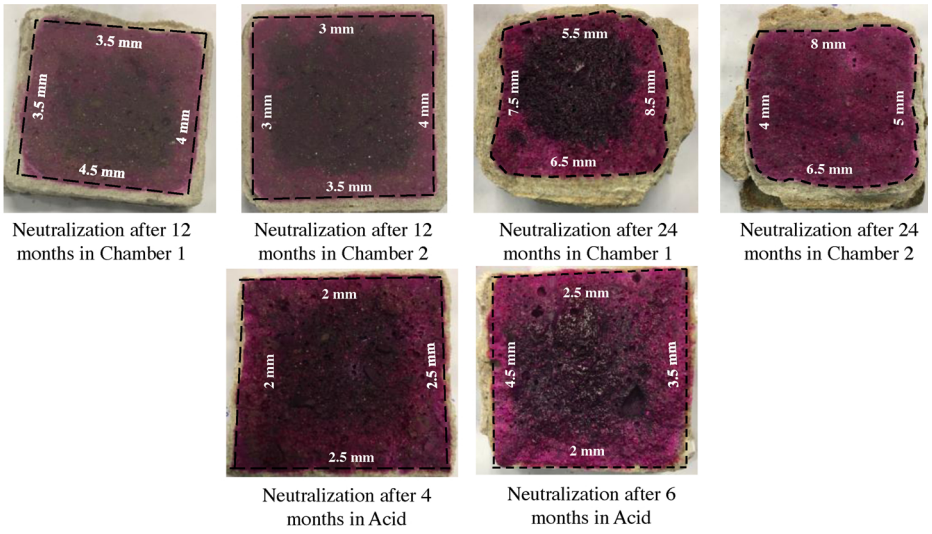

(a) Neutralization depth of SRPCm

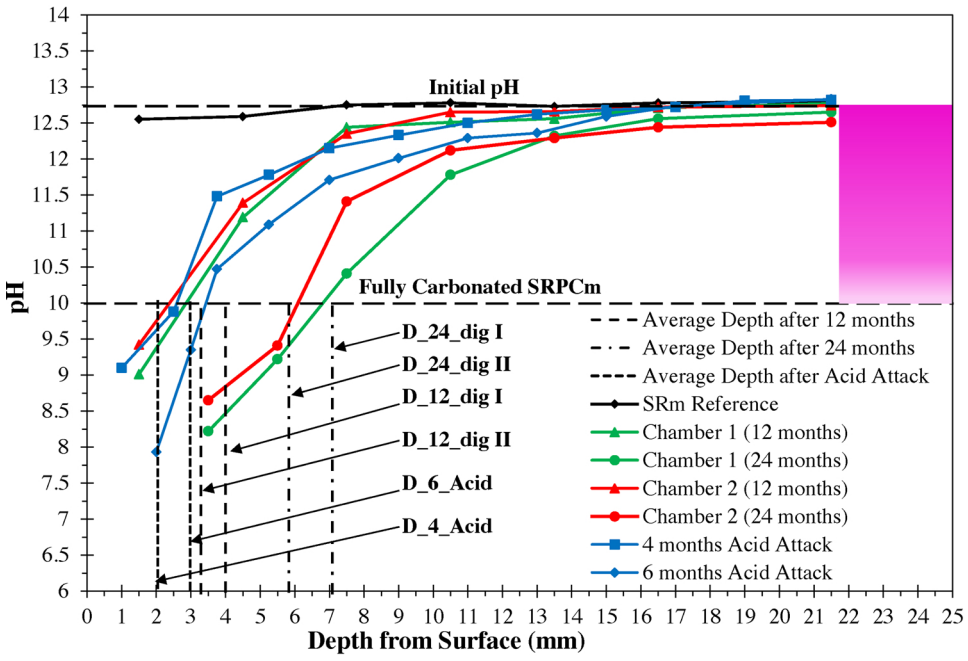

(b) SRPCm pH profile

Fig. 8. Depth of neutralization and profile of pH of SRPCm after infield sewer environments and sulphuric acid solution exposure [36].

shown with a vertical line on the pH profile graph.

In sulphuric acidic solution, the estimated depth of neutralization depth of FA-GPm was 7 mm and 9.2 mm after 4 and 6 months of exposure, respectively. A steep gradient in pH was observed for these mortars close to exposure surface, indicating the depth up to which the matrix is affected. Results are consistent with the neutralization depth measured using phenolphthalein. However, a large difference is observed between infield environment and sulphuric acid attack due to the difference in the exposure conditions. In natural sewer environment simultaneous carbonation and acidification of H_2S leads to the neutralization of the whole matrix whereas, in sulphuric acid experiment, this loss in alkalinity is due to the transport mechanism and diffusion of proton and sulphate anion from acid solution.

The minimum pH of 10 was estimated for carbonated portland cement by previous researchers [63–65], which designate the fully neutralized pH of SRPCm (Fig. 8(b)). After one year of exposure in chamber 2 and 1, the average neutralization depth measured was around 3.3 mm–4.0 mm, respectively. This estimated depth was much reduced compared to FA-GPm. This depth of neutralization was increased from 0.28 mm per month estimated during the first year to a rate of 0.31 mm per month in chamber 1. This light increase in neutralization rate was due to the rise in annual average H_2S concentration in chamber 1. Fig. 8(b) shows the profile of pH of SRPC mortar after 1 and 2 years of exposure in the sewer environment, in addition pH of SRPCm specimen is also shown after 4 and 6 months of sulphuric acid exposure [36]. Due to simultaneous carbonation and attack of H_2S in the sewage environment, a pH drop of almost 3.5 was estimated after 1 year of exposure. Furthermore, removal of 2–3 mm of surface was also considered while plotting the pH profiles and depth of neutralization after 12–24 months of exposure. The lowermost pH value measured was

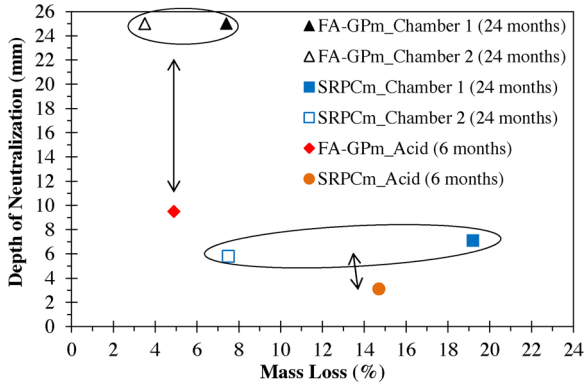

Fig. 9. Neutralization depth in relation to mass loss for both FA-GPm and SRPCm under two aggressive conditions of infield sewer and 1.5 % sulphuric acid.

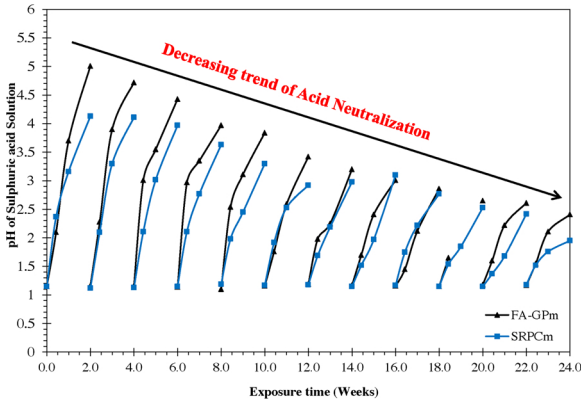

Fig. 10. pH of the sulphuric acid solution during the immersion of FA-GPm and SRPCm.

around 8.2 and 8.65 in chamber 1 and 2, respectively, after 2 years of exposure. Moreover, with the increase in depth the pH of these specimens gradually converged to the initial pH observed on control specimens, in contrast to FA-GPm. Further, this increase in neutralization depth in specimens collected after 24 months from chamber 1 can be linked to the rise in annual average H_2S concentration which was much greater compared to chamber 2. After the sulphuric acid attack for the duration of 6 months, the loss in pH was almost around 4.7 in SRPCm which was less than FA-GPm (~5.3). In addition, around 1 mm of loss in surface material was also considered while estimating the pH profile and neutralization depth. The pH profile of SRPCm against acid exposure depicts a lowest pH value of around 7.83 followed by 8.95, which represents the heavily corroded zone of 4 mm. Further, it is also seen that in case of SRPCm under both experiments, most of the region which had experienced loss in alkalinity is lost. In contrast, the matrix of FA-GPm which had experienced major loss in alkalinity was still intact.

Fig. 9 represents the relationship between alkalinity loss in terms of depth of neutralization and mass loss for both types of mortar for infield and acid exposure. The behaviour of these mixes is grouped into four categories, i.e. FA-GPm and SRPCm against infield exposure and acid attack. It is worth noting that, the geopolymer mix under both aggressive conditions experienced smaller loss in mass with much greater loss in alkalinity. In contrast, SRPCm specimens showed major loss in mass with insignificant loss in pH and alkalinity within the core of the specimen. This highlights the difference in mechanisms of degradation which is linked to the porosity of theses mortars. Breakdown of N-A-S-H gel matrix in an acidic environment with low calcium content, results in the formation of durable siliceous framework with higher porosity but resistant to further acid attack [29,66–68]. On the other hand, the degradation of SRPCm initiates with the formation of calcium sulphate salts followed by matrix dissociation and removal of highly degraded layers due to crack propagation. As a result, FA-GPm performed better in terms of loss in mass, whereas, SRPCm showed better neutralization resistance. In addition, it is worth pointing out that the degradation mechanisms under acid exposure are very different from infield exposure. This leads to a much higher neutralization depth observed in sewer environment in comparison with sulphuric acid (Fig. 9). In natural sewer, the initial alkalinity loss was due to concurrent acidification of H_2S and diffusion of carbon dioxide into the matrix which followed Fick's Law [69]. This is followed by the disintegration of the matrix due to MICC stage II (growth of biotic colonies) causing further reduction in pH. In contrast, the neutralization by acid solution was due to the transport mechanism, penetration of sulphate anion and H^+ from sulphuric acid solution and leaching of the Ca^{2+}, Al^{3+} and Na^+ [28,70], which is limited to the development of diffusion flux, rapid neutralization reaction between proton, and capillary suction of acid through the pores [53].

3.5. Neutralization of acid by leaching

The matrix neutralization and leaching in the solution of H_2SO_4 (having reference pH of 1.05 ± 0.02) was estimated periodically throughout 2 weeks cycles. Fig. 10 shows the recorded acid solution pH from the start of the experiment till 6 months of exposure; during this time duration the solution was renewed fortnightly to attain the initial pH value. This initial pH of the H_2SO_4 solution increased from 1.15 ± 0.02 to more than 4.0 for both FA-GPm and SRPCm within the first two cycles. This increase in pH can be linked to the leaching of ions from the matrix and the consumption of proton (H^+) by the mortars [56]. This led to the neutralization of proton (H^+) and transfer of sulphate (SO_4^{-2}) into the matrix. This increase in pH is dependent on the number of renewal cycles and the type of the binder specimen exposed. It is also seen that for both mixes, the acid neutralization and the rise in pH keeps decreasing with every subsequent attack cycle (Fig. 10). This reduction in maximum pH indicates the decline in decalcification of SRPCm [71], reduction in consumption of proton and leaching of alkali, and similarly reduction in de-alumination followed by removal of alkali from FA-GPm. It is also observed that initially within the first two cycles, more than 99 % of acid was consumed and H^+ was neutralized for both mixes. Afterwards, the neutralization potential was reduced to 94.3 % and 83.1 % in FA-GPm and SRPCm, respectively after 6 months of exposure. This means that Ca^{2+} and Na^{1+}, Al^{3+} has already been removed from the matrix near exposure surface due to decalcification, loss of alkali and dealumination, respectively, during the previous cycle. This is followed by the deterioration of deeper layers, as observed by Gruyaert et al. [71]. It is also observed that in each cycle the neutralization was much higher in acid solution containing FA-GPm in comparison with SRPCm, however, afterwards the rise in pH of the acid solution was reduced and almost equivalent for both mixes (Fig. 10). This higher neutralization of acid solution by FA-GPm means greater percentage of ions leaching (ejection of aluminium and ion exchange between proton and alkali) from the matrix as compared to SRPCm, linked to the neutralization and disintegration of the matrix.

Fig. 11 represents the elemental analysis using ICP-MS of the acid solution to estimate the leaching of calcium, aluminium, silicon, sodium, iron, magnesium and potassium from FA-GPm and SRPCm during the first 14 days exposure. Negligible concentration of iron, magnesium and potassium (< 200 mg/L) was measured for both FA-GPm and SRPCm. Significant leaching of sodium, aluminium, calcium, and silicon were identified with 2580, 712, 630, and 385 mg/L concentration, respectively after 14 days immersion of FA-GPm mix. A sudden rise in quantity of Na^+ from 0 to more than 2000 mg/L was detected within the first week of exposure indicating the ion exchange of alkali with

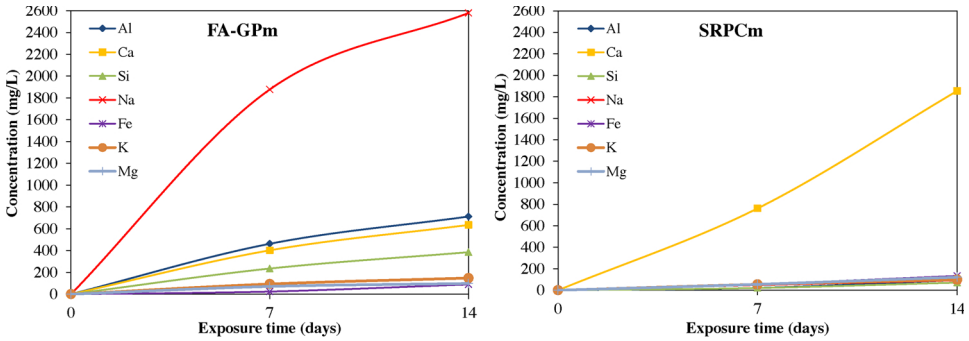

Fig. 11. Concentration of elements leached in to the acid solution during FA-GPm and SRPCm 14 days' exposure.

proton (H^+) due to acid attack. This rise in sodium and silicon concentration in geopolymer mix was also due to the initial high concentration of the alkaline activator solution (sodium silicate and sodium hydroxide) [60]. The rise in concentration of Al^{3+} was also identified within the acid solution having FA-GPm which is due to the release of aluminium from Si-O-Al gel matrix from deteriorated zone following acid attack [27,72]. However, in case of SRPCm negligible rise in concentration of sodium, aluminium and silicon was observed (< 100 mg/L). Finally, around 1255 mg/L concentration of calcium was measured after 14 days of exposure. The quantity of calcium was steadily rising (Fig. 11(b)). In contrast, calcium leaching was moderate and stabilized to around 630 mg/L in FA-GPm acid solution. This is due to the low calcium content of FA-GPm matrix. However, by standardizing the overall concentration of ions leached from the matrix of FA-GPm and SRPCm compared to initial concentrations within the matrix, it is observed that around 0.97 % and 0.43 % of Ca^{2+} leached out, respectively. This indicated that with reference to initial composition more calcium is leached from FA-GPm matrix as compared to the SRPCm matrix. Further, the concentration of Ca^{+2} measured in SRPCm acid solution does not represent the full range of leaching, since the counter diffusing anion of sulphate (SO_4^{2-}) reacts with these cations to precipitate gypsum within the deteriorated zone, blocking further diffusion. Similarly, by standardizing the Al^{3+} leachates, it is observed that around 0.98 % and 0.67 % of aluminium leached from FA-GPm and SRPCm, respectively in the first cycle. This greater concentration of Al within the solution was due to the poor reactivity of Al with sulphate anion compared to Ca.

3.6. Microstructural characterization

To identify and characterize the microstructural deteriorations scanning electron microscopy (SEM) with energy dispersive X-Ray (EDX) analysis, X-Ray diffraction (XRD) and fourier transform infrared (FTIR) spectroscopy were carried out. The quality of aggregate-matrix bond is also observed within the matrix which is one the primary factor behind durability and strength of concrete [73,74].

3.6.1. X-Ray diffraction (XRD) analysis

Fig. 12 shows the XRD pattern of FA-GPm with respect to depth (every 3 mm) after exposure to sewer chamber for 2 years and H_2SO_4 solution for 6 months. Each powder analysed was collected over the depth of 3 mm starting from the surface of exposure. The reference FA-GPm exhibited the occurrence of quartz from sand (SiO_2, PDF# 01-074-9758) and mullite ($Al_{4.7}Si_{1.2}O_{9.5}$, PDF# 98-020-2159) owing to the presence of unreacted fly ash particles. Moreover, the development of amorphous sodium aluminosilicate hydrate (N-A-S-H) gel was also observed which shifted the initial amorphous hump between 15 and 30° and indicating the alumina-silicate glass formation to 20 and 32° [75,76]. Further, due to the 15 % GGBFS, a broad peak at 29° is observed, which represents the formation of hybrid matrix of N-C-A-S-H as result of the dissolution, coagulation, and reorganisation of fly ash and slag blend [77–79]. After 2 years of exposure to infield exposure, geopolymer sample showed the presence of natron ($Na_2CO_3.10H_2O$, PDF# 04-016-5072) at 16.5° and 29.6°, and calcite ($CaCO_3$, PDF# 01-086-2342) at 29.4° due to carbonation. Prominent peak of gypsum ($CaSO_4.2H_2O$, PDF# 04-009-3817) is observed at 11.7°, 20.8°, 29.1° and 31.2° up to 12 mm and 9 mm depth in specimens from chamber 1 and 2, respectively. This gypsum crystallization within FA-GPm matrix is formed as a result of dissociation and decalcification of calcium based gel matrix [29]. In addition, the broad peak of N-C-A-S-H was no longer identified up to 12 mm depth in chamber 1. In addition, no peak of Thernadite (Na_2SO_4) at 32° is seen, which was observed previously by authors after 2 years of sewer exposure [35]. The XRD results of FA-GPm after exposure to sulphuric acid have shown almost similar patterns in comparison to infield assessment. Peaks of mullite and quartz are observed throughout the depth. However, peaks of gypsum were prominent up to 6 mm depth. In addition, the broad peak of amorphous N-C-A-S-H gel at 29° also reappears after 6 mm depth from exposure.

The XRD of SRPCm mortar (before exposure) displays the mineral Quartz (SiO_2, PDF# 01-074-9758) at 20.8°, 26.6°, 36.5°, 50.1° and 60°, Portlandite ($Ca(OH)_2$, PDF# 01-070-5492) at 18.1°, 36.2° and Calcium Silicate Hydrate (C-S-H) (PDF# 00-033-0306) at 29.4° (Fig. 13). After 2 years of infield sewer exposure, dissociation of primary hydrates and crystallization of secondary minerals were observed within the microstructure due to the reaction with sulphate from acid. Since the exterior surface was reduced by about 2 mm due to material loss, the first layer of powder goes up to 6 mm depth. Prominent peak of gypsum was identified at 11.6° up to 10 mm depth in SRPCm from chamber 1 (see Eqs. (3) and (4) [20,80]). In chamber 2, this peak of $CaSO_4{\cdot}2H_2O$ was noticeable up to 5 mm depth. In addition, delayed ettringite was also formed beyond 6 mm depth at 9.1° 2θ, due to the reaction of gypsum and mono-sulfoaluminate, as shown in Eq. (5) [81]. However within the initial corroding layer (< 6 mm), ettringite mineral was not identified. This might be due to the fast reaction thermodynamics of gypsum crystallization within region of high sulphate anion concentration [19] and low pH of the corroding layer which restrict the crystallization of ettringite [58]. Further, peak of calcite was also identified up to at 10 mm depth; however, this carbonation product was not seen beyond this depth. Similar to infield exposure, the SRPCm after exposure to H_2SO_4 solution have shown the disappearance of calcium hydroxide and calcium silicate hydrate within 3 mm depth from exposure. Gypsum and quartz were the only prominent phases observed in the corroded layer of SRPCm after acid exposure.

3.6.2. Fourier transform infrared (FTIR) spectroscopy

FTIR analysis can identify the depth of deterioration by detecting

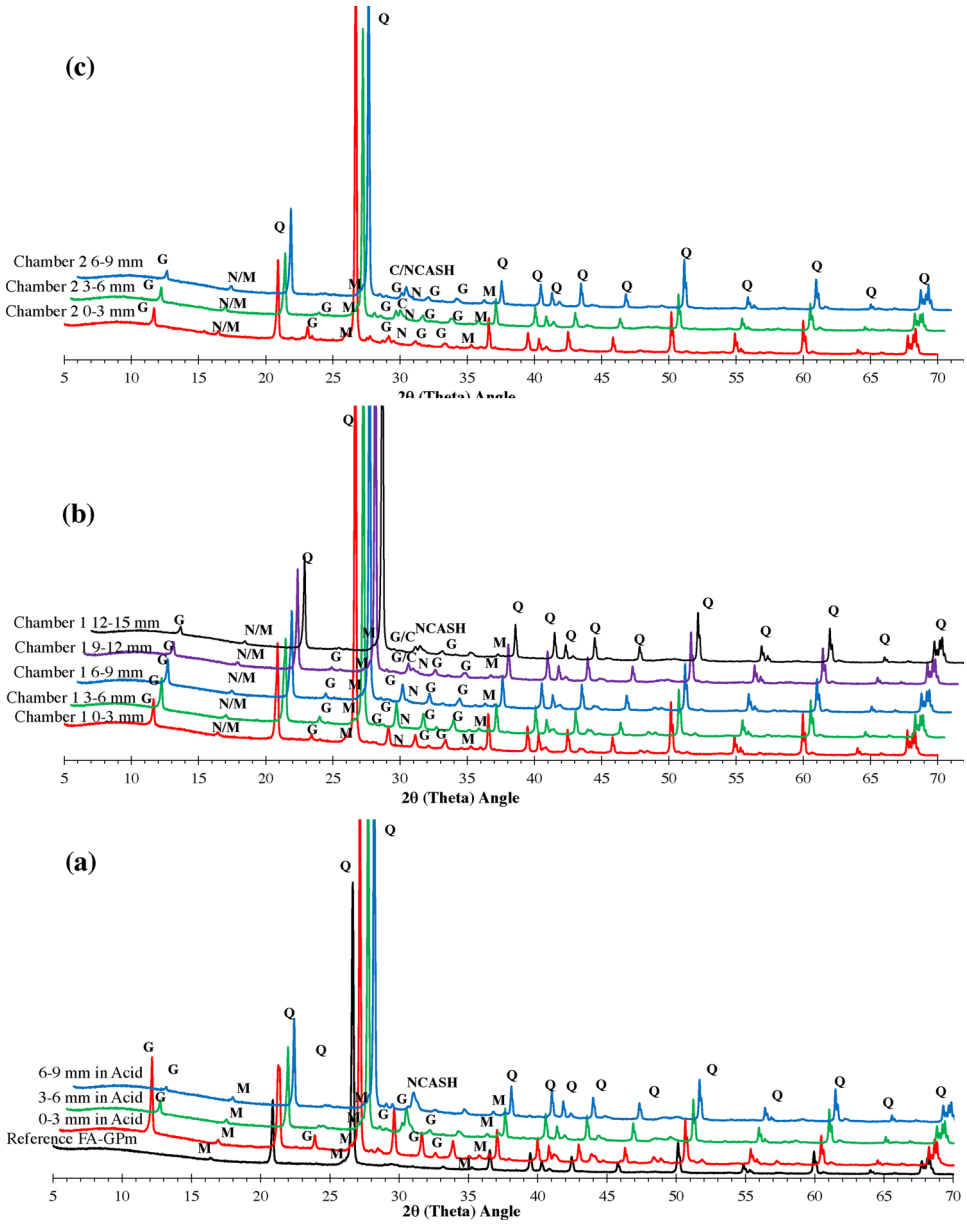

Fig. 12. XRD patterns of FA-GPm a) After 6 months in acid exposure; b) after 24 months in aggressive sewer (chamber 1) and c) after 24 months in aggressive sewer (chamber 2). Q – Quartz, M – Mullite, G – Gypsum, C – Calcite, N – Natron, N-C-A-S-H – Sodium rich aluminosilicate hydrate.

the peaks of infrared at different wavenumbers formed as a result of symmetric and asymmetric stretching and bending due to the presence of carbonate $(CO_3)^{-2}$ and sulphate $(SO_4)^{-2}$ groups [82]. Moreover, it can also highlight the spectral variations of primary phases present within the reference specimen. Fig. 14(a) represents the variation in FTIR spectra of reference FA-GPm with respect to exposure conditions (24 months in chamber 1 and 2 sewer and 6 months in sulphuric acid) and depth from exposed surface (every 3 mm). In reference FA-GP, major bands were identified at 998 cm^{-1}, 885 cm^{-1}, 798 cm^{-1}, 785 cm^{-1}, and 690 cm^{-1}. Asymmetric stretching vibration of Si-O-Si within the N-A-S-H or N-C-A-S-H gel matrix is identified at ~998 cm^{-1} [25,83,84]. In fly ash and slag blended alkali activated systems, this vibration varies from 960 to 1100 cm^{-1}, with higher wavenumber representing crosslinked siliceous N-A-S-H gel whereas lower wavenumber represents highly substituted C-S-H gel [84,85]. Symmetric stretching generated by Si-O-Si bond is located at ~690 cm^{-1}. Further, band at around 850 – 890 cm^{-1} are assigned to the stretching of Si – OH, whereas wavelength between 780 – 800 cm^{-1} represents the O—Si—O bonds within quartz crystalline phase [70]. Exposure to the natural sewer and 1.5 % acid solution shows a slight shifting of the main peak to higher wavenumber suggesting deterioration [25]. In chamber 1, the asymmetric stretching of Si-O-Si in FA-GPm is shifted to around 1058 cm^{-1} up to around 6 mm depth. This is shifted back to its original position at around 12 mm depth. Similarly, in chamber 2 and sulphuric acid solution this shift was observed but only up to 6 mm depth. This shift indicates the increase in Si/Al ratio in FA-GPm representing highly siliceous gel matrix formed after de-alumination of binding gel [25]. In addition, stretching of O—H and bending of H—O—H indicating bonded H_2O at around ~3406 cm^{-1} and ~1610 cm^{-1}, respectively confirming the presence of gypsum within the matrix [70]. Moreover, a peak at ~660 cm^{-1} was also identified within the deteriorated region of FA-GPm up to 12 mm in chamber 1, 6 mm in chamber 2 and acid solution, representing the weaker stretching band of $(SO_4)^{2-}$ group [29]. A peak of the C—O functional group is also identified at ~1450 cm^{-1} representing the carbonation of the matrix [82,86].

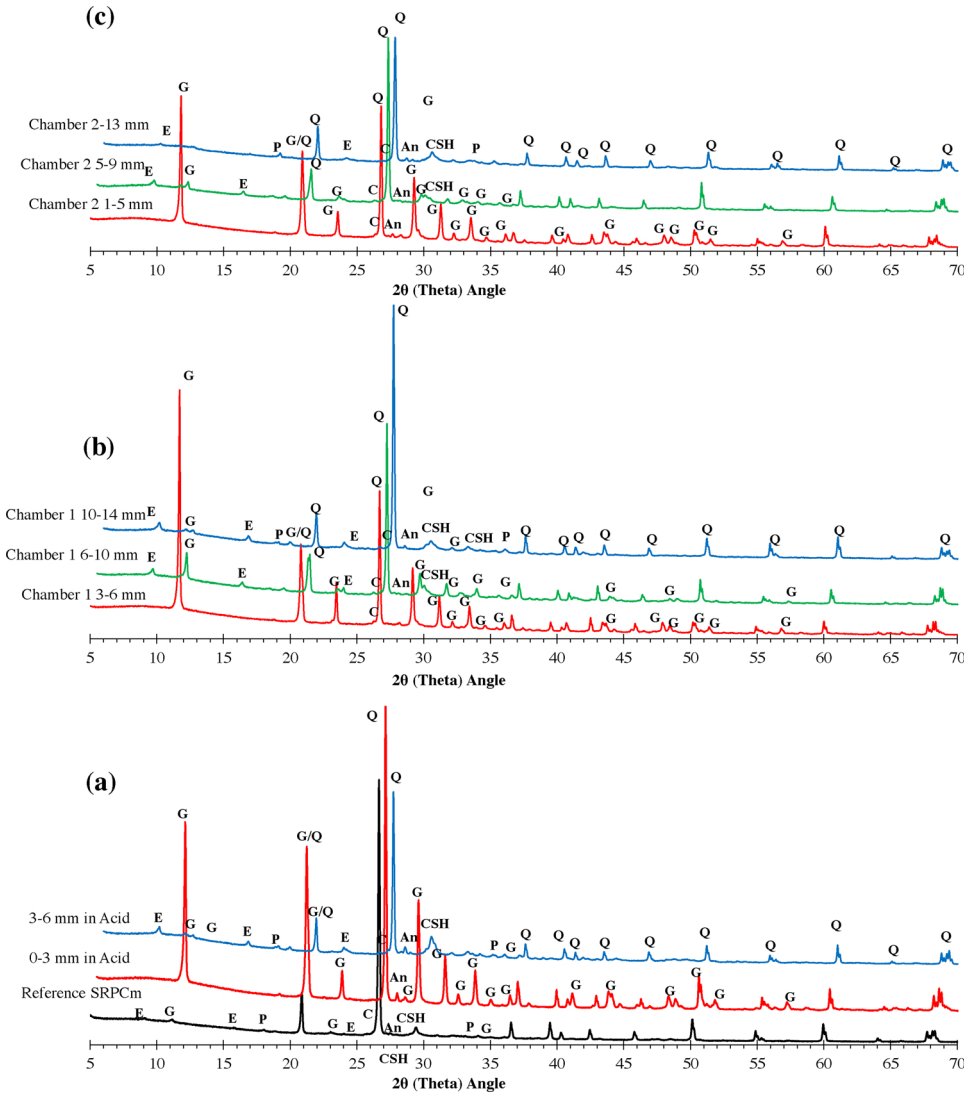

Fig. 13. XRD patterns of SRPCm a) After 6 months acid exposure; b) after 24 months in aggressive sewer (chamber 1) and c) after 24 months in aggressive sewer (chamber 2). (Q – Quartz, G – Gypsum, P – Portlandite, C – Calcite, An – Anorthite, C-S-H – Calcium silicate hydrate, E – Ettringite [36].

Fig. 14(b) represents the FTIR spectra of SRPCm before and after deterioration in aggressive infield environment and H_2SO_4 solution. The major bands identified in reference SRPCm are located at 1160 cm^{-1}, 1075 cm^{-1}, 960 cm^{-1}, 798 cm^{-1}, 780 cm^{-1} and 690 cm^{-1}. The asymmetric stretching vibration of silicon-oxygen bond was identified at 1075 cm^{-1} to 1055 cm^{-1} representing C—S—H gel and quartz in SRPCm [87]. The peak depicting Ca bonded with oxygen within C—S—H was observed at 960 cm^{-1} and shifting of this band to higher value indicate the dissociation of C—S—H matrix [70]. Moreover, the peak centred at 690 cm^{-1} was also identified representing the bending vibration of O-Si-O and Al-O [88]. After 2 years of exposure, shifting in reference bands was identified beside the creation of new bands. Crystallization of calcite results in noticeable formation of peak at 1481 cm^{-1} representing the asymmetric stretching vibrations [86]. However, beyond 10 mm the intensity of this peak (identified within 1410–1415 cm^{-1}) was reduced representing reduction in carbonation (see XRD and Neutralization results). This slight shift in the peak of calcite shows that different polymorphs of calcite was crystallized having different frequencies [89]. Bending vibrations of these carbonate phases is identified at around 875 cm^{-1} and 855 cm^{-1}. Similarly, FTIR spectra in chamber 2 also show the formation of carbonate mineral beyond 5 mm, however, the peaks are not that noticeable. Moreover, chemically bonded H_2O molecule was also identified at 1685 cm^{-1} and 1626 cm^{-1}, representing the bending bands. In addition, stretching of O—H bond is observed at 3560 cm^{-1} to 3410 cm^{-1} [90,91]. In addition, a noticeable peak of sulphate group was also observed at 1120 cm^{-1} wavelength which represents the stretching vibrations, followed by a weaker stretching band at 660 cm^{-1} up to around 10 and 9 mm depth in SRPCm from chamber 1 and 2, respectively [29,91]. This indicates that formation of $CaSO_4.2H_2O$ modifies the SRPCm microstructure within the deteriorated region. Further, decalcification of C—S—H gel after exposure was identified as a shift in main peak at 960 cm^{-1} to wavelength of 998 – 1001 cm^{-1} within 6 mm depth and are consistent with XRD results. After exposure to acid solution, almost similar dissociation of C—S—H gel matrix is observed with the formation of gypsum and band movement of primary peak to a higher wavelength of 1120 cm^{-1}. This deterioration of C—S—H binder was more pronounced at 3 mm depth. At 6 mm depth, peak at 960 cm^{-1} reappeared which represents the vibrations of oxygen within C—S—H gel matrix with the reduction in peak at 1120 cm^{-1}. This indicates less crystallization of sulphate mineral beyond 6 mm depth supporting the results presented in XRD analysis, pH profile and confirms the deterioration depth of SRPCm after infield and H_2SO_4 solution exposure.

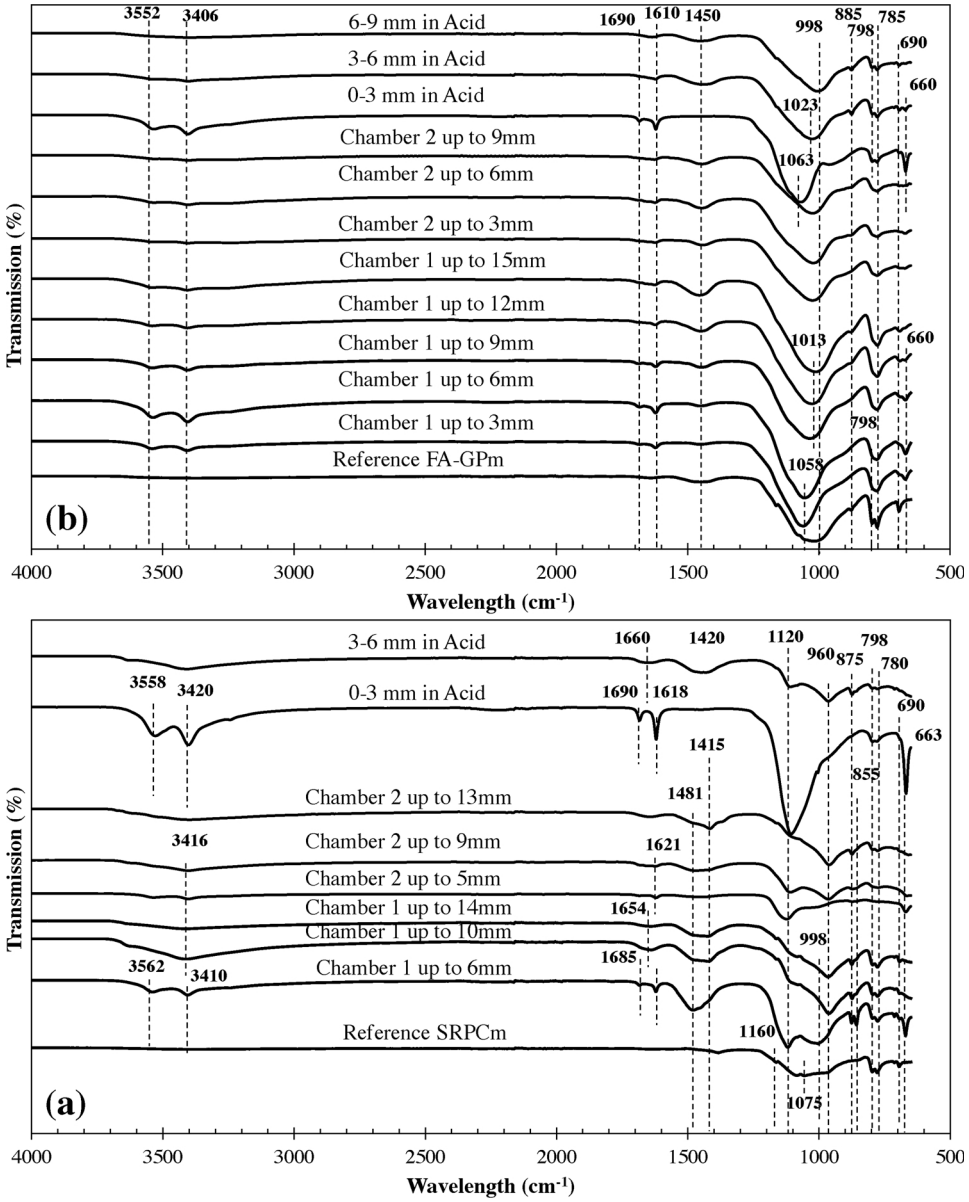

Fig. 14. FTIR spectra with reference to depth from exposure surface, after 2 years in natural infield environment and 6 months in H_2SO_4 solution; a) SRPCm and b) FA-GPm.

3.6.3. Scanning electron microscopy (SEM) with Energy Dispersive X-Ray (EDX) analysis

3.6.3.1. Exposure to infield sewer environment. EDX point analysis with mapping is performed with respect to depth. The Si/Al, Ca/Si and Na/Si elemental ratios with associated standard deviation (SD) for both mixes are presented with respect to the chamber and depth in Table 5. Multiple numbers of EDX points and blocks which ranges from 10 to 15 and 8 to 12, respectively, were analysed at various locations of the SEM image by avoiding the quartz aggregate to assess the dissolution of the geopolymer gel matrix, decalcification of C-S-H matrix, crystallization of minerals and penetration of sulphate within the matrix, as performed by previous researchers [29,70,92–94]. Initial Si/Al and Na/Si ratio of the geopolymer matrix was estimated to be around 3.25 ± 0.44 and 0.25 ± 0.03, respectively, before exposure. Due to the low quantity of GGBFS, the concentration of calcium in FA-GPm is low with an initial Ca/Si ratio of around 0.12 ± 0.2 [95]. This indicates that majority of the gel matrix is composed of crosslinked siliceous N-A-S-H gel with coexistence of minor quantity of hybrid N-C-A-S-H gel at some particular locations [96,97]. Similarly, Si/Al and Ca/Si ratios of SRPCm were also measured before exposure and were around 6.4 ± 1.5 and 3.2 ± 0.6, respectively.

After 2 years of exposure, the concentration of sodium (Na) in FA-GPm was immensely reduced, resulting in a drop of Na/Si ratio from 0.25 to 0.003 within the exposure region (up to 12 mm). Similarly, beside the loss in alkalinity, partial de-alumination of N-A-S-H gel matrix is also observed within the matrix of FA-GPm leading to the rapid rise in Si/Al ratio. This aluminum substitution causes microstructural changes from gel formwork to silica gel followed by an increase in porosity [98]. However, no complete erosion or matrix disintegration was observed, as seen in C—S—H gel matrix [29,60]. Further, the hybrid N-C-A-S-H gel experienced similar dissolution reactions and decalcification [29]. This resulted in the crystallization of gypsum within those locations. The loss of alkali was observed throughout the depth of FA-GPm specimens from the surface of exposure till core matrix. However, minor dealumination was only identified up to 12 mm depth from exposure surface, indicating that the Si-O-Al bond is still intact within the matrix beyond 12 mm. This loss of alkali from the gel matrix initiated with the crystallization of sodium

Table 5
Elemental mass ratios (Si/Al, Ca/Si, Na/Si and Ca/S) of FA-GPm and SRPCm obtained with EDX spectroscopy with respect to depth from exposure surface.

Elemental mass ratios	FA-GPm Initial Wt. % ratio (SD)	FA-GPm			SRPCm Initial Wt. % ratio (SD)	SRPCm		
		Location	Cham 1 Wt.% ratio (SD)	Cham 2 Wt.% ratio (SD)		Location	Cham 1 Wt.% ratio (SD)	Cham 2 Wt.% ratio (SD)
Si/Al (SD)	3.25 (0.44)	0–12 mm 12 mm onwards	5.8 (1.8) 3.5 (0.8)	3.1 (1.3) 2.7 (0.9)	6.4 (1.5)	2–6 mm 6 mm onwards	2.5 (0.56) 3.1 (0.62)	3.0 (0.5) 3.7 (0.36)
Ca/Si (SD)	0.11 (0.2)	0–12 mm 12 mm onwards	0.045 (0.08) 0.069 (0.06)	0.063 (0.12) 0.077 (0.16)	3.2 (0.6)	2–6mm 6 mm onwards	0.88 (0.38) 1.41 (0.51)	0.98 (0.47) 1.5 (0.66)
Na/Si (SD)	0.25 (0.03)	0–12 mm 12 mm onwards	0.003 (0.003) 0.05 (0.006)	0.032 (0.05) 0.08 (0.07)	–	– –	– –	– –
Ca/S (SD)	15.9 (0.22)	0–12 mm 12 mm onwards	0.45 (0.2) 4.9 (0.45)	0.78 (0.12) 3.6 (0.5)	47.9 (0.58)	2–6mm 6 mm onwards	2.9 (0.34) 15.9 (0.9)	4.68 (0.56) 15.2 (0.87)

sulphate salt as a transition, observed by the authors after 12 months of infield exposure [35], followed by leaching of these secondary hydrates. Dissociation of SRPCm matrix initiated with the decalcification of calcium based hydrates (C—S—H and portlandite) followed by the crystallization of gypsum [47,99]. This led to a reduction in Ca/Si ratio by 72.5 % from 3.2 to 0.88 over 4 mm depth from exposure surface. Further, it is also observed that the FA-GPm and SRPCm specimens were more severely affected with the dissociation of matrix, loss of alkali and decalcification in chamber 1 as compared to chamber 2, due to the rise in annual average concentration of H_2S in chamber 1, making it more aggressive compared to chamber 2.

SEM images and EDX spectrum of FA-GPm matrix after exposure to the sewer environment are shown in Figs. 15 and 16, respectively. Geopolymer specimens from both chambers show a dissociation of binding gel matrix. Fig. 15(a) displays the creation of voids and gaps within the microstructure of FA-GPm from chamber 1 near interface with aggregate. Similarly, voids and gaps were also observed in the matrix of FA-GPm from chamber 2 (Fig. 15(b)). This rise in porosity is linked to the major loss in compressive strength and bulk density observed on the geopolymer specimens. Beside the dissolution of geopolymer matrix, some precipitation of gypsum was also observed within the microstructure of FA-GPm at few localized regions near exposure surface (Fig. 15(c)). This is further identified by performing EDX analysis at these locations and the result is shown in Fig. 16. The microstructure of FA-GPm was also analysed beyond 12 mm depth from exposure surface using SEM with EDX (Fig. 15(d)). Beside the loss of alkalinity from the gel matrix, no major dealumination was observed. This indicates that the framework of cross-linked N-A-S-H gel matrix is slightly disoriented with the loss of alkali. However, the matrix is still intact with no major signs of dissolution. EDX analysis is also performed within this region to estimate the Si/Al ratio and formation of different minerals (Fig. 16). The localized crystallization of gypsum was identified having high concentration of sulphur and low concentration of aluminium, indicating decalcification and dealumination of the gel matrix. The Si/Al ratio within the core was around 3.5, which is almost equivalent to the initial reference specimen, confirming no dissociation of the aluminosilicate gel matrix. Elemental analysis using EDX mapping technique on FA-GPm specimen from chamber 1 and 2 is shown in Fig. 15(e) and (f), respectively. Beside the localized precipitation of gypsum, no alkali was observed within the matrix, confirming the loss of alkalinity. However, partial dealumination within the matrix was seen, indicating limited transformation of gel framework to amorphous silica gel structure, due to the penetration of acid. This transformation of the gel matrix leads to a rise in porosity [98].

Figs. 17 and 18 represent the SEM imagery and EDX mapping of SRPCm specimens after 2 years of exposure. Extensive penetration of sulphur was seen within the matrix, which led to the disintegration of portlandite and C-S-H matrix, beside the widespread precipitation of gypsum. This also results in the degradation of matrix by forming gaps at the aggregate-matrix interface (Fig. 17(a) and (d)). This caused the development of cracks, as shown in Fig. 17(b). Beside the crystallization of gypsum, nucleation of ettringite was also observed leading to further internal stresses within the matrix. The EDX block analysis of these minerals was also performed and results are shown in Fig. 18. The extensive penetration of sulphur and crystallization of gypsum are also analyzed using EDX mapping technique on specimens from both chambers (Fig. 17(e) and (f)). It is observed that the pattern of crystallization of sulphate mineral appears in the form of parallel layers against exposure surface. In addition, beside the crystallization of gypsum, silicon and aluminum were completely depleted in these layers of deterioration. Moreover beyond 6 mm depth, nucleation of ettringite was also confirmed within the matrix using EDX analysis.

3.6.3.2. Exposure to sulphuric acid. Corroded microstructure of FA-GPm and SRPCm was examined using SEM and EDX analysis after 6 months of exposure to acid solution and results are presented in Figs. 19 and 20, respectively. In FA-GPm, dissolution of N-A-S-H gel matrix was observed at some locations after the penetration of hydronium (H^+) cation and sulphate anion from the acid solution. This led to the formation of pores and gaps within the gel matrix followed by localized formation of gypsum, as shown in Fig. 19(a) and (b). Moreover, the crystalline phases which were identified after infield sewage exposure were not observed. Since the matrix of FA-GPm was rich in silicon and aluminium which was polymerized into the alkali-activated aluminosilicate gel, no extensive crystallization of gypsum was observed. Fig. 19(c) and (d) shows the block analysis results using EDX technique within the corroded matrix of FA-GPm where formation of minerals was observed. EDX spectrum showed the presence of Si, Al and O as major elements whereas, Ca and S is observed only at two locations confirming no uniform distribution of gypsum, as observed by Allahverdi and Škvara [27]. In addition, as the acid attack progresses, the alkali leaches out from the geopolymer matrix followed by the cation-exchange reaction with the H_3O^+. This drop in alkali concentration is observed using EDX analysis considering Na/Si ratio which was drastically reduced to (<0.01) molar ratios within deteriorated zones (Fig. 19(d)). Further, by comparing the concentration of aluminium and silicon by calculating Si/Al ratios at all four locations, it is observed that this molar ratio varies from 5.8 to 1.8. This means that relatively uniform matrix of Al-O-Si experienced disintegration into small parts with localized gypsum crystallization separating the matrix (Fig. 19(e)). This indicates that the cross-linked aluminosilicate gel matrix is disoriented after the loss of alkali and formation of gypsum; however, the presence of aluminium confirms that no major de-alumination occurred, confirming that gel matrix is

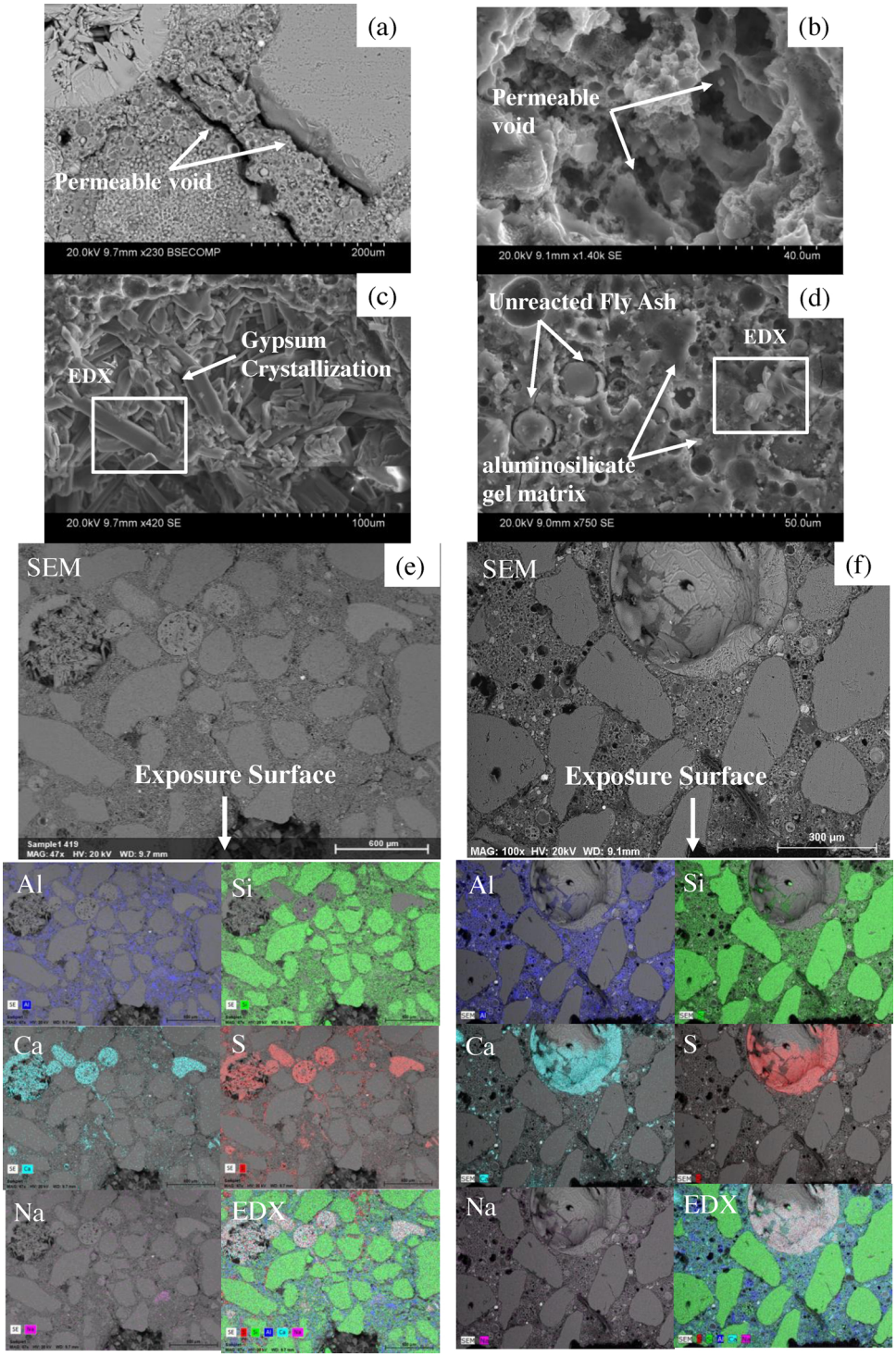

Fig. 15. SEM images with EDX elemental mapping of FA-GPm after exposure to aggressive sewer environment in chamber 1 and 2 for 24 months; Permeable voids and gaps in FA-GPm a) from chamber 1, b) from chamber 2, c) crystallization of gypsum extracted from chamber 1 (with selected region for EDX), d) undisturbed matrix within core layers (with selected region for EDX). EDX mapping of FA-GPm (arrow showing exposure surface) displaying the distribution of elements (Si, Al, Ca, S, Na) in e) chamber 1, and f) chamber 2.

still intact. Further, the concentration of sulphur varies from 0.1 to 13% by weight depending on the location indicating localized crystallization of sulphate. Fig. 19 also shows the results of the elemental analysis (Ca, Na, Si, Al and S) using EDX mapping technique on FA-GPm specimen after exposure to acid solution. In the initial 2.2 mm corroded region of FA-GPm localized formation of gypsum was observed due to the decalcification of hybrid N-C-A-S-H and the leaching of Na^+. This loss of alkalinity results in the major reduction of pH observed within the matrix. Beside this deposition of gypsum within the matrix, aluminium is also observed in disintegrated form with varying concentrations at different locations representing the disorientation of Al-O-Si polymer matrix. However, no severe loss of alumina was seen, indicating no major transformation of gel framework to amorphous silica gel structure.

The deteriorated matrix of SRPCm after 6 months of exposure to acid attack represents a more generalized decalcification of C-S-H

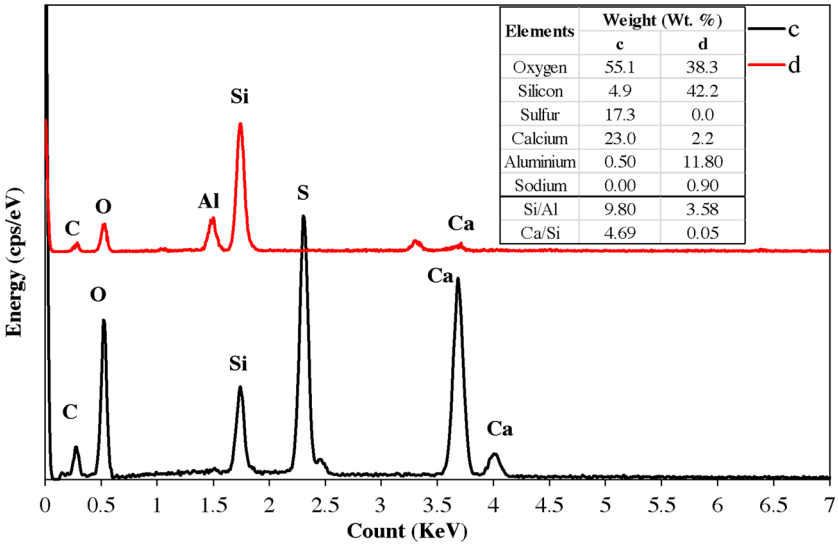

Elements	Weight (Wt. %)	
	c	d
Oxygen	55.1	38.3
Silicon	4.9	42.2
Sulfur	17.3	0.0
Calcium	23.0	2.2
Aluminium	0.50	11.80
Sodium	0.00	0.90
Si/Al	9.80	3.58
Ca/Si	4.69	0.05

Fig. 16. EDX spectroscopy with elemental analysis at selected region within FA-GPm matrix designated in Fig. 15(c) and (d).

matrix followed by the crystallization of gypsum (Fig. 20(b) and (c)). This C-S-H dissociation and nucleation of gypsum not only weakens the matrix of SRPCm but also introduces expansive stresses leading to the widening of aggregate-matrix interface (Fig. 20(a)). Elemental distribution of Ca, Si, Al and S was also performed using EDX analysis and results are shown in Fig. 20. Sulphur concentration within the matrix was represented in red colour spots and it was observed that SRPCm matrix experienced a uniform rise in concentration of sulphur. This sulphate anion reacted with the calcium leaching towards the solution to form gypsum crystals within these corroded layers leading to the formation of micro-cracks and loss of surface material. In addition, slight depletion of aluminium and silicon is also seen. Since no sodium based activator was used in SRPCm, the Na content was negligible; hence the distribution of sodium is not shown. Further, the deteriorated region and depth of penetration observed using EDX analysis for both mixes was quite similar to the depth of neutralization estimated using phenolphthalein indicator solution (see Figs. 9 and 10).

After performing detailed microstructural assessment using SEM with EDX analysis on both FA-GPm and SRPCm from chemically induced acid degradation and aggressive sewer exposure, significant differences were observed. In FA-GPm, it seems that the dissociation after attack of acid solution was not that extensive within the geopolymer gel matrix and crystallization of gypsum was observed up to only 4.5 mm of depth, whereas in natural conditions the disintegration and dealumination of the matrix was identified up to 12 mm. Further, in both experimental programs, leaching of alkali was observed, which can be considered as the initiation of deterioration of geopolymer under acidic environment. Similarly, since the matrix of geopolymer is composed of hybrid N-C-A-S-H due to the addition of slag, localized nucleation of gypsum was seen under both aggressive conditions. The minerology and morphology of precipitates within the deteriorated matrix of SRPCm was identical after the exposure to infield and H_2SO_4 solution. Moreover, the deterioration of C-S-H within the degraded matrix also led to the development of micro-cracks and crystallization of secondary sulphate minerals. However, the pattern of this sulphate minerals precipitation and mechanism of corrosion was different. In sulphuric acid solution experiment, the deteriorated matrix was severely corroded after the diffusion of sulphate from H_2SO_4 solution causing deterioration of binding gel matrix and extensive nucleation of $CaSO_4.2H_2O$. In comparison, the deterioration mechanism in natural sewer started with the development of micro porosity due to the biodegradation and acidification by H_2S causing further penetration of sulphate and using the Ca from C-S-H gel matrix to precipitate $CaSO_4.2H_2O$ between micro-cracks (Fig. 17). Moreover, separate layers were formed within the microstructure up to 6 mm depth, in addition to the surface loss of 2 − 3 mm at exposure. This crystallization pattern of $CaSO_4.2H_2O$ and breakdown of C-S-H matrix was unlike that observed after acid exposure, where slow and steady microstructural disintegration was originated and progressed into the matrix. Furthermore, the ratio of Ca/Si measured within the deteriorated regions surrounding the crystallization of $CaSO_4.2H_2O$ layers were low (< 1.0), in contrast to that observed in specimen after acid attack.

3.7. Degradation mechanics with respect to exposure conditions

The mechanism of corrosion of FA-GPm and SRPCm are quite different with respect to exposure conditions. Fig. 21 shows the schematic of degradation process within the matrix of these mortars based on the leachate analysis, microstructural studies and physical deterioration observed. After exposure to sewer environment chambers with high concentration of H_2S gas, multistage MICC process initiates with the reduction of surface pH due to combined carbonation and acidification of H_2S. After the reduction of surface pH to more desirable pH (< 9.0), growth of sulphur oxidizing microorganisms initiates within the matrix of mortar which leads to the disintegration of the matrix after oxidizing H_2S gas from environment to sulphuric acid [14]. In case of low-calcium FA-GPm, carbonation and H_2S acidification leads to the cation-exchange reaction and forms alkali-carbonates or alkali-sulphates [35], which is followed by leaching of these salts. This leaching results in the lowering of the pH to a completely undesirable value posing major threats to core matrix.

In case of SRPCm, continuous diffusion of H_2S gas and biogenic acid production leads to the decalcification and dissociation of calcium based primary hydrates (C-S-H, $Ca(OH)_2$) by crystallizing gypsum. This deteriorated zone is extended inwards from the exposure surface till the region up to which sulphates are crystallized and binder gel is disintegrated. However, since the matrix of low-calcium FA-GPm is more porous than C-S-H based matrix in SRPCm, the depth of corrosion due to sulphate crystallization was slightly superior in FA-GPm. Moreover, higher content of calcium within the matrix of SRPCm leads to more nucleation of gypsum causing internal expansive stresses resulting in the disintegration of the microstructure.

Exposure to acid results in an increase in porosity due to the coarsening of pores near the exposure surface [53]. This accelerates the diffusion of sulphate towards the intact matrix. The SO_4^{2-} from the acid penetrates the matrix through the porosity within the ITZ to react

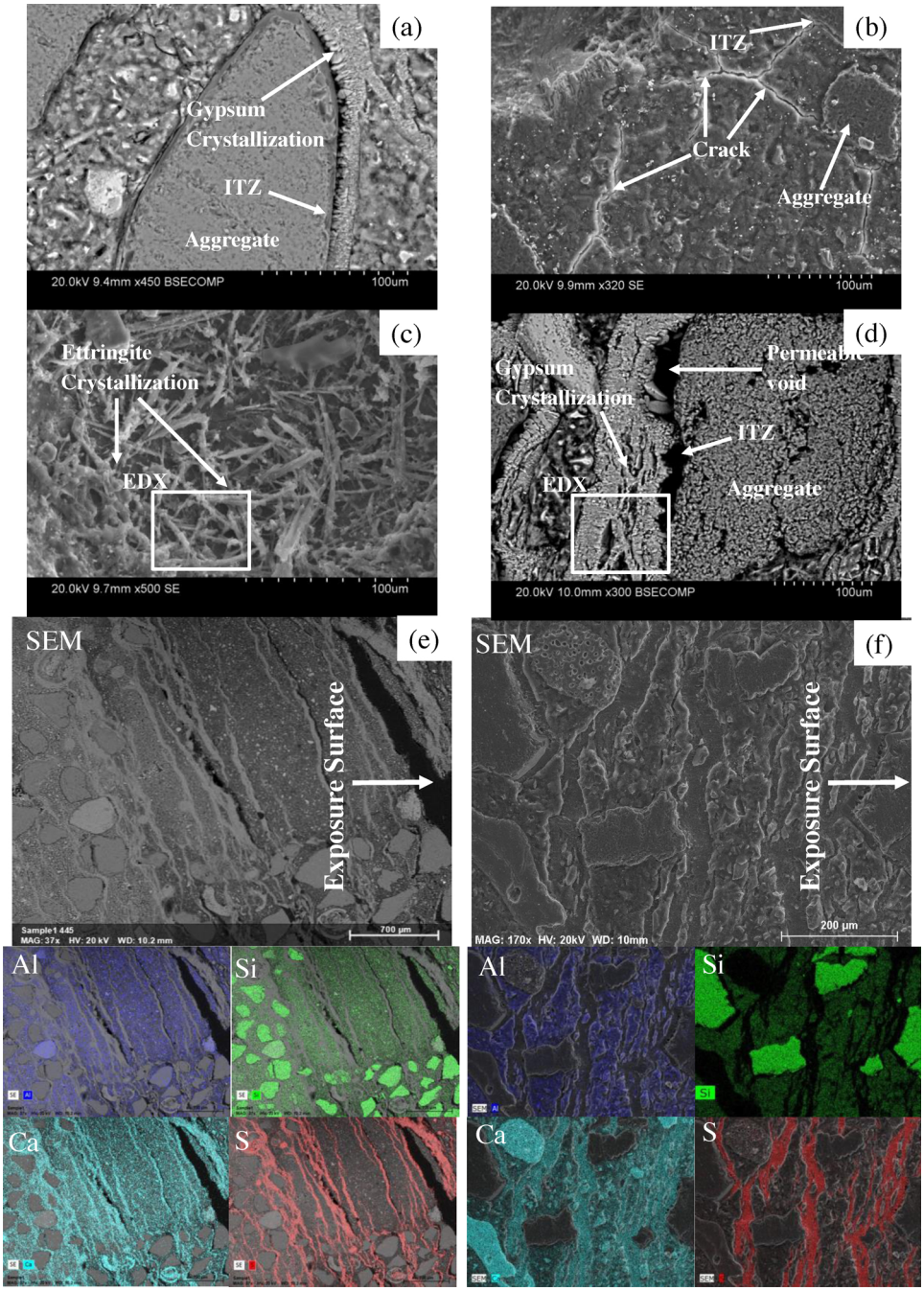

Fig. 17. SEM images with EDX mapping of SRPCm after exposure to aggressive sewer environment in chamber 1 and 2 for 24 months; a) Gypsum crystallization at ITZ from chamber 1, b) crack propagation, c) crystallization of ettringite in SRPCm extracted from chamber 1 (with selected region for EDX), d) Permeable voids and crystallization of gypsum near ITZ in SRPCm extracted from chamber 2 (with selected region for EDX). EDX mapping of SRPCm (arrow showing exposure surface) displaying the distribution of elements (Si, Al, Ca, S) in e) chamber 1, and f) chamber 2.

with hydrates. Expansive salts were formed which leads to the deterioration of the microstructure and causes weakening of the matrix-aggregate bond [56]. Therefore, the depth of corrosion within geopolymer and Portland cement mortars is due to the transport mechanism and diffusion of sulphate and proton from sulphuric acid solution [28,70]. Since, this migration of acid is limited to the development of diffusion flux and capillary suction of acid through the pores [53], a lower deterioration depth was observed in FA-GPm and SRPCm as compared to infield experiment. However, the capillary suction and diffusion flux of sulphate anion reduces with the crystallization of sulphate minerals within the microstructure of these mortars [53,55]. This deterioration was restricted up to the transition region, identified by a yellowish brown zone next to undamaged core (Fig. 21). This transition zone was identified only in SRPCm and was limited to 0.5–1.5 mm thickness having pH ranging from 10 to 11 with a decrease in cations concentration (Na^+, Ca^{2+}, Al^{3+}). This decrease in cations is due to the development of diffusion flux from the matrix towards the acid solution [53]. Further, the $(OH)^{1-}$ diffused from the matrix also counter react with the H^+ available in the H_2SO_4 solution and increases the acid pH (neutralize).

The microscopic analysis of FA-GPm showed no distinctive transition zone indicating that no restriction to diffusion of sulphate was present within the matrix. This facilitates the ion exchange between the N-A-S-H matrix and the acid solution which is followed by de-

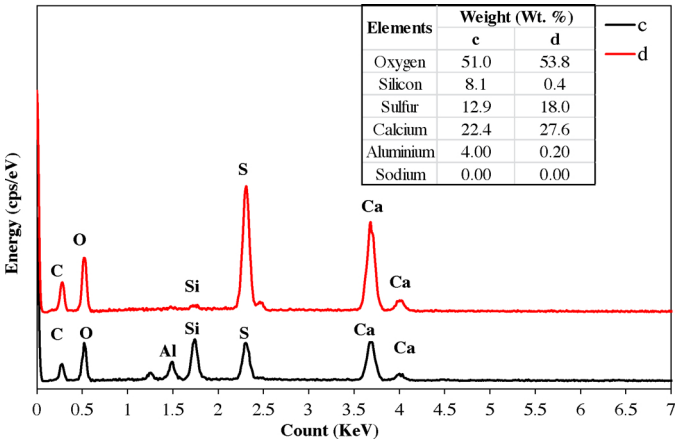

Fig. 18. EDX spectroscopy with elemental analysis at selected region within SRPCm matrix designated in Fig. 17(c) and (d).

alumination of Si-O-Al bond. This was followed by the disintegration of the aluminosilicate gel as well as decalcification by diffusing proton and sulphate. This leads to the formation of highly siliceous framework resistant to further acid attack, hence the deteriorated matrix remains intact with minor loss of surface material [25,72]. Moreover in comparison with SRPCm, only localized precipitation of gypsum within FA-GPm matrix was identified, indicating that no major internal stresses were developed. As a result, no extensive cracking and loss of material was observed in FA-GPm, contrary to SRPCm.

3.8. Corrosion depth

The depth of corrosion is another very important indicator used to assess the durability of mortars. The surface deterioration by acid attack and natural MICC was estimated using a method suggested by Lloyd et al. [30]. However, considering only the loss of surface material is not ideal to estimate the corrosion depth [60], Since the loss of surface material was negligible in case of FA-GPm with major reduction of alkalinity and greater penetration of sulphate. Hence, the depth of corrosion was estimated by considering the loss of surface material, and deterioration observed in microstructure by SEM, XRD and FTIR for both types of mixes after exposure to both sewer chamber and H_2SO_4 solution.

For FA-GPm, the presence of permeable voids, dissociation of matrix due to dealumination of N-A-S-H gel and crystallization of gypsum due to decalcification of N-C-A-S-H binder were the primary indicators up to which the depth of corrosion is considered. Similarly for SRPCm, the corrosion depth is estimated based on the presence of gypsum and formation of micro-cracks within the matrix. Table 6 shows the measured depth of corrosion within specimens exposed to these chambers and the previous infield case studies of OPC concrete for comparison purpose. Table 6 shows that the depths of deterioration estimated in FA-GPm and SRPCm are comparable to previous infield case studies.

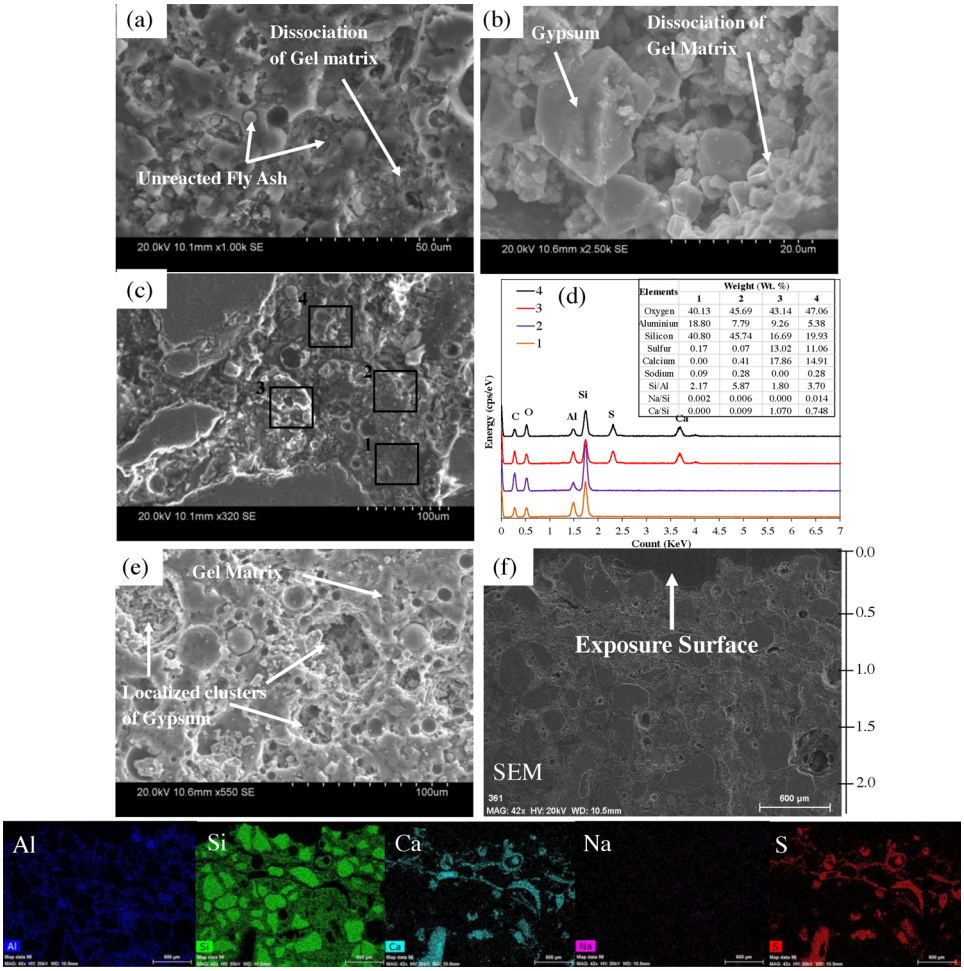

Fig. 19. SEM images with EDX elemental mapping of FA-GPm after 6 months of sulphuric acid solution exposure; a) Dissociation of Gel matrix, b) Gypsum crystallization, c) localized regions of gypsum crystallization within gel matrix, and d) EDX mapping of FA-GPm (arrow showing exposure surface) with elemental analysis showing distribution of elements (Al, Si, Ca, Na, S).

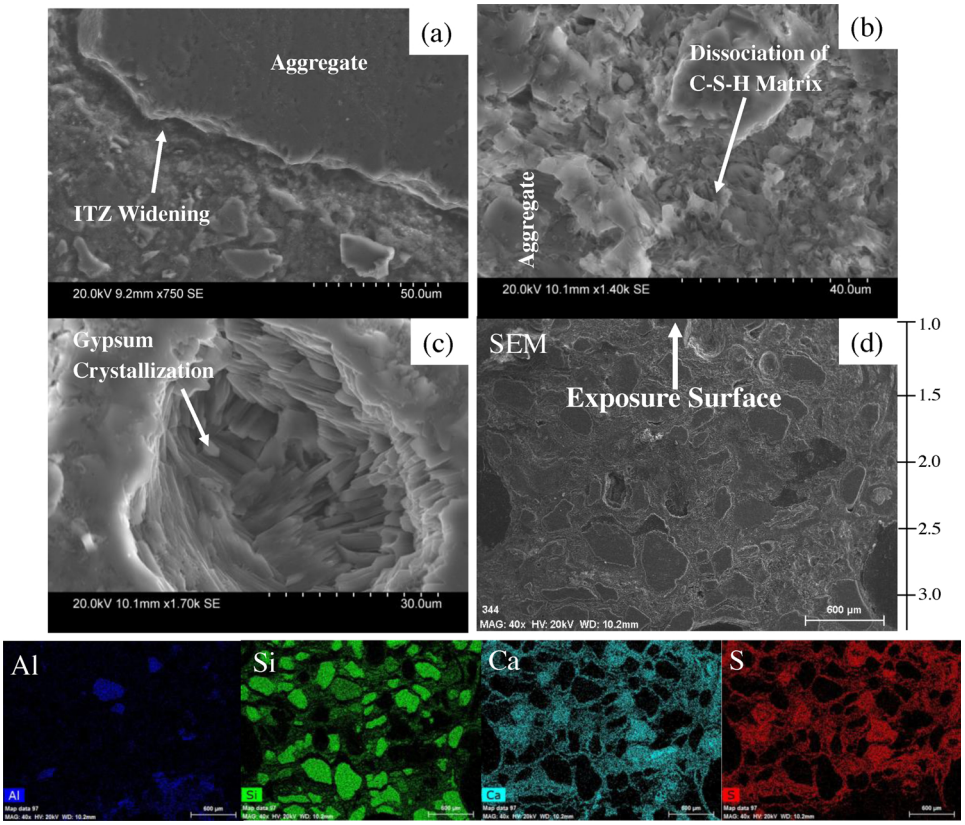

Fig. 20. SEM images with EDX mapping of SRPCm after 6 months of exposure to sulphuric acid solution; a) ITZ widening, b) dissociation of C-S-H matrix, c) crystallization of gypsum, and d) EDX mapping of SRPCm (arrow showing exposure surface) with elemental analysis showing distribution of elements (Al, Si, Ca, S).

Fig. 22 represents the corrosion depths of FA-GPm and SRPCm after deterioration in aggressive sewer and sulphuric acid solution. Each point represents the average of three depths of deterioration measured using SEM with EDX, XRD and FTIR spectroscopy. It is observed that the depth of corrosion was only 1.1–1.2 times higher in FA-GPm compared to SRPCm after 24 months in natural sewer conditions. This difference in depth of degradation between FA-GPm and SRPCm after exposure to acid solution was around 34 %. Further, it was also observed that corrosion was much advanced in the specimens extracted from digester I as compared to digester II indicating the effect of higher H_2S concentration and temperature. This slightly higher degradation in FA-GPm can be linked to the permeability facilitating the diffusion of acid into the matrix. Since the characteristic of the FA-GPm matrix is such that volume of permeable pores is much higher, after exposure to acid solution, the degradation front indicated by the penetration of sulphate was more advanced in FA-GPm. Moreover, the diffusion of acid was restricted in SRPCm after the generalized precipitation of gypsum within the microstructure limiting further penetration to some extent. However, it was observed that the deterioration of matrix was more detrimental in SRPCm compared to the FA-GPm, due to the dissociation of C-S-H gel, which leads to the development of expansive stresses causing the loss of surface material. In contrast, FA-GPm matrix, even after the de-alumination of aluminosilicate gel, remains intact due to the formation of acid resistant amorphous siliceous gel [25,29].

3.9. Summary of the results

The investigation of deterioration mechanism within FA-GPm and SRPCm mortars using different microstructural techniques (XRD, FTIR, SEM with EDX) and assessment of different physical parameters like surface pH, depth of neutralization, loss in mass and strength, depth of deterioration and increase in porosity aided in ranking the binders after two years of exposure in two different on-site conditions and six months in acid solution. The performances of these binders are presented with respect to these parameters in a kiviat diagram (Fig. 23). Higher number in this diagram means less corrosion depth, neutralization of matrix, increase in porosity, reduction in strength, mass, and surface pH. It is estimated that FA-GPm and SRPCm binders were more deteriorated after exposure to chamber I compared to chamber II. Furthermore, the FA-GPm specimens showed higher neutralization depth and loss in alkalinity compared to SRPCm. However, the reduction in mass and strength was greater in SRPCm.

3.10. Development of linear models to predict corrosion

The experimental data obtained from the natural sewer environment was used to develop multivariable first order linear models for time-dependent deterioration of mortars. Linearity of corrosion was supported by both short term exposure tests in laboratory [100,101] and long term experiments conducted in sewer environments with varying concentration of H_2S gas [38,102]. These developed mathematical equations will facilitate the estimation of corrosion of mortars based on the environmental conditions and types of binder used. Since the deterioration of these mortars was very much dependent on the concentration of H_2S in the natural sewer environment hence, H_2S is considered as a primary controlling factor. The concentration of H_2S experienced major fluctuations due to the dynamics in sewage flow and variations in exposure conditions, therefore average concentration of H_2S was estimated over the whole exposure time for both chambers. In addition, exposure time was also considered as another independent variable. During the exposure time span, deterioration and loss in pH was also observed even the concentration of H_2S was minimal (<10 ppm). This was due to additional chemical reactions such as carbonations within the natural sewer environment. Furthermore, the initiation of corrosion was also estimated by Jiang et al. [102] and it was observed that the rate of deterioration was enhanced with the

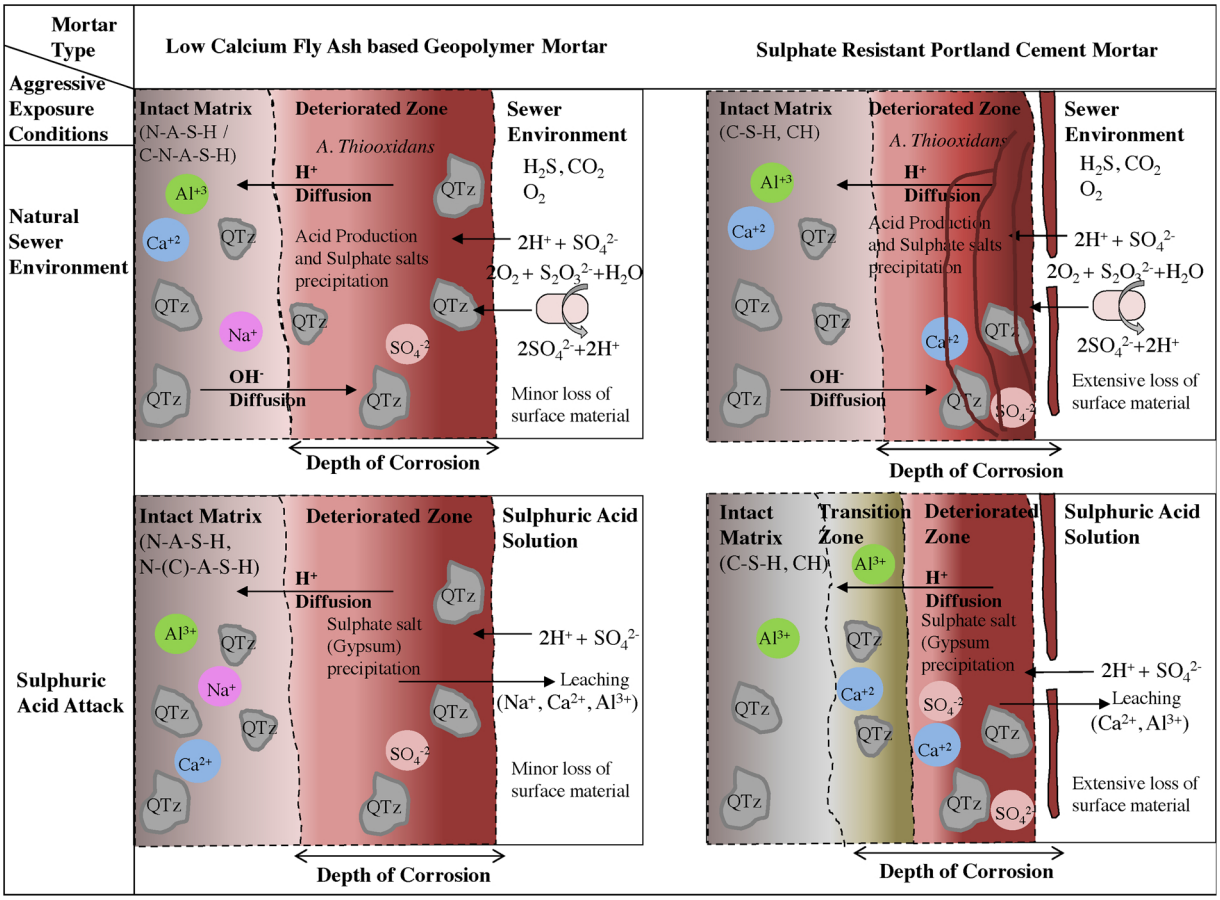

Fig. 21. Schematic model of deterioration mechanism in FA-GPm and SRPCm matrix for two aggressive exposure conditions of sewer environment and sulphuric acid solution.

Table 6
Measured corrosion depth per annum (mm/yr) within FA-GPm, SRPCm and concretes exposed to sewers pipes in previous case studies.

Field conditions	Corrosion depth (mm/yr)
FA-GPm in Chamber 1 (NHWTP)	6
FA-GPm in Chamber 2 (NHWTP)	3.5
SRPCm in Chamber 1 (NHWTP)	4.5
SRPCm in Chamber 2 (NHWTP)	3
Grengg et al. [2]	4
Wells and Melchers [38] – Perth A	5
Wells and Melchers [38] – Melbourne A	1
Wells and Melchers [38] – Sydney A	1.5

increase in temperature. Wells et al. [38], while modelling the deterioration of concrete based on field observations, also estimated the variation in temperature and included the gas phase temperature in his model. Hence, temperature was also considered as another independent variable in the models. For both FA-GPm and SRPCm, linear models were developed for depth of corrosion, neutralization depth, surface pH and weight loss as a function of average H_2S concentration (ppm), temperature (°C) and exposure time (days). Regression analysis was performed to develop these empirical equations. The generic form of multivariable linear regression model is given in Eq. (6).

$$Y = \beta_o + \beta_1 x_1 + \beta_2 x_2 + \beta_3 x_3 \quad (6)$$

Where, Y represents the dependent variable (Corrosion depth, Surface pH, neutralization depth and loss in mass), β, represents the model coefficients and x are the independent variables (H_2S concentration, temperature and exposure time). β_o represents the y-intercept of the model and describes the expected values of response variable when all independent variables are zero. β_1, β_2 and β_3 represent the rate of change of dependent variable with a unit increase in independent variable by keeping the other variable constant. These selected corrosion models are presented in Table 6. H_2S gas concentration (ppm), temperature (°C) and exposure time (days) are represented by C_{H2S}, T and E_T, respectively. Fitting was carried out by minimising the sum of squared residuals also known as coefficient of determination (R^2). This R^2 is actually the proportion of total variation in the response that is explained by the variable prediction in a simple regression model and represents the proportion of the sum of square of error about their independent variable [103]. Results indicate that all parameters are significant at 95 % confidence level and can explain the variation reasonably well. Limitations for these deterioration models are the results of the natural conditions i.e. average H_2S concentration, average temperature variations and duration of exposure.

The goodness-of-fit for the corrosion depth (C) (that is, coefficient of determination; R^2) is approximately 0.95 and 0.99 for FA-GPm and SRPCm, suggesting that the model captures about 95%–99% of the variation in the data for these mixes, respectively. Similarly other models also have high predictive ability (Table 7). In addition, the 95 % confidence interval is also calculated for these models and is mentioned in Table 6. Significance F value were also obtained, which must be less than 0.05 [103]. Further, the confidence interval values does not contain zero which indicates that there exists a linear relationship between dependent and independent variables [103]. This shows that data is statistically significant at 95 % confidence level and the model explains the deviation reasonably well. In addition, the coefficient of these models depicts the relation of concentration of H_2S, temperature and exposure duration with physical parameters. In case of corrosion depth, the concentration of H_2S shows a positive correlation for these two

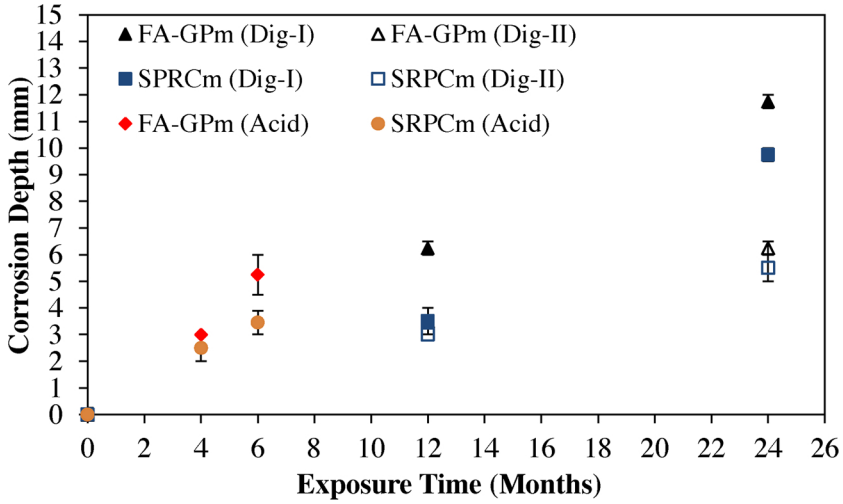

Fig. 22. Corrosion depth of FA-GPm and SRPCm with respect to exposure time for two aggressive conditions of sewer environment and sulphuric acid solution.

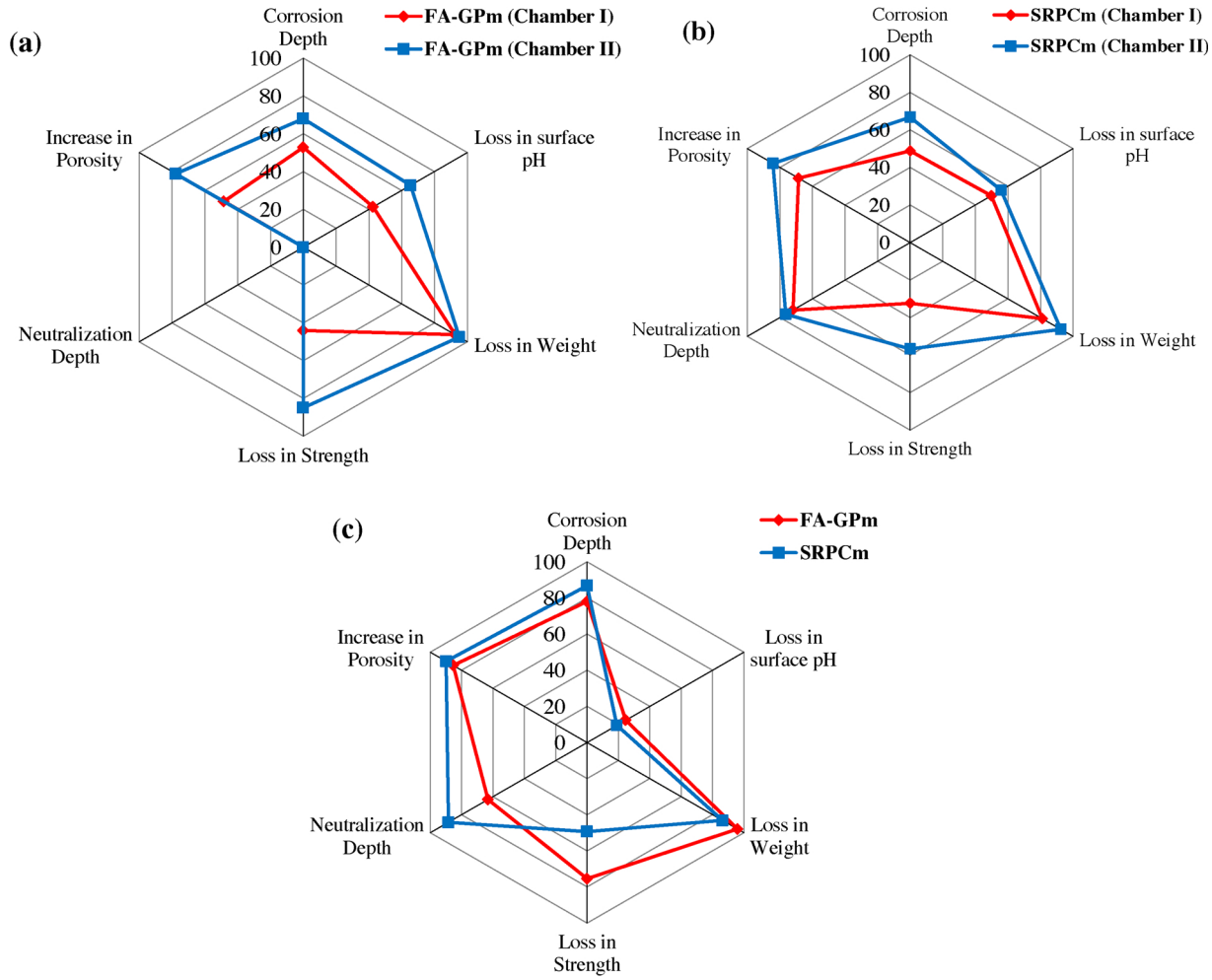

Fig. 23. Performance of binders with respect to natural sewage environment (chambers I and II) and after acid attack; (a) FA-GPm, (b) SRPCm, (c) exposure to acid solution.

mixes, indicating that a unit increase (that is, one ppm) in H_2S tends to increase the corrosion depth (mm) by respective coefficient. Further, similar behaviour are shown for exposure time which can be interpreted in the same way. In contrast, opposite relation are shown for H_2S concentration and exposure time with surface pH (S_{pH}), indicating that a unit increase in these variables will cause a reduction in surface pH. Models for mass (M) variations can also be interpreted similarly to surface pH models. Further, the effect of temperature on these models varies with the mix type and physical parameter. Moreover, the depth of neutralization (N) showed that for SRPCm all three independent variables are positively associated suggesting a proportional relationship, unlike FA-GPm. R^2 values obtained for SRPCm is more than 0.95

Table 7
Summary of Corrosion models for FA-GPm and SRPCm.

Type of Mortar	Physical Parameter	Response Variable	Linear Regression Model	R^2	Limitation of variable	95 % Confidence values		Sig. F
						Lower	Upper	
FA-GPm	Corrosion Depth (mm)	C	$0.122C_{H_2S} + 0.13T + 0.008E_T - 3.96$	0.97	$0 < C_{H_2S} \leq 53\,ppm$ $155 \leq E_T \leq 735\,days$ $13.7 < T \leq 34.1°C$	$\begin{Bmatrix} Intercept = -11.8 \\ E_T = 0.0044 \\ T = -0.2186 \\ C_{H_2S} = 0.0518 \end{Bmatrix}$	$\begin{Bmatrix} Intercept = 3.88 \\ E_T = 0.0112 \\ T = 0.473 \\ C_{H_2S} = 0.192 \end{Bmatrix}$	0.0003
	Surface pH (pH unit)	S_{pH}	$-0.061C_{H_2S} + 0.009T - 0.0014E_T + 9.37$	0.89		$\begin{Bmatrix} Intercept = 4.36 \\ E_T = -0.0036 \\ T = -0.212 \\ C_{H_2S} = -0.1064 \end{Bmatrix}$	$\begin{Bmatrix} Intercept = 14.4 \\ E_T = 0.0007 \\ T = 0.23 \\ C_{H_2S} = -0.0164 \end{Bmatrix}$	0.008
	Mass Loss (%)	M	$-0.091C_{H_2S} + 0.077T - 0.006E_T + 0.13$	0.95		$\begin{Bmatrix} Intercept = -6.8 \\ E_T = -0.0092 \\ T = -0.226 \\ C_{H_2S} = -0.153 \end{Bmatrix}$	$\begin{Bmatrix} Intercept = 7.02 \\ E_T = -0.0032 \\ T = 0.3816 \\ C_{H_2S} = -0.029 \end{Bmatrix}$	0.0008
	Neutralization Depth (mm)	N	$-0.09C_{H_2S} + 1.26T + 0.02E_T - 15.5$	0.74		$\begin{Bmatrix} Intercept = -56.6 \\ E_T = 0.0014 \\ T = -0.546 \\ C_{H_2S} = -0.463 \end{Bmatrix}$	$\begin{Bmatrix} Intercept = 25.6 \\ E_T = 0.037 \\ T = 3.1 \\ C_{H_2S} = 0.27 \end{Bmatrix}$	0.06
SRPCm	Corrosion Depth (mm)	C	$0.194C_{H_2S} - 0.09T + 0.0067E_T - 0.339$	0.99	$0 < C_{H_2S} \leq 53\,ppm$ $155 \leq E_T \leq 735\,days$ $13.7 < T \leq 34.1°C$	$\begin{Bmatrix} Intercept = -5.07 \\ E_T = 0.0045 \\ T = -0.299 \\ C_{H_2S} = 0.151 \end{Bmatrix}$	$\begin{Bmatrix} Intercept = 4.4 \\ E_T = 0.0087 \\ T = 0.1174 \\ C_{H_2S} = 0.2365 \end{Bmatrix}$	1.5×10^{-5}
	Surface pH (pH unit)	S_{pH}	$-0.013C_{H_2S} - 0.022T - 0.0052E_T + 11.6$	0.98		$\begin{Bmatrix} Intercept = 8.95 \\ E_T = -0.0064 \\ T = -0.138 \\ C_{H_2S} = -0.0368 \end{Bmatrix}$	$\begin{Bmatrix} Intercept = 14.23 \\ E_T = -0.0041 \\ T = 0.094 \\ C_{H_2S} = 0.0105 \end{Bmatrix}$	9.9×10^{-5}
	Mass Loss (%)	M	$-0.38C_{H_2S} + 0.26T - 0.005E_T + 0.362$	0.95		$\begin{Bmatrix} Intercept = -18.2 \\ E_T = -0.014 \\ T = -0.555 \\ C_{H_2S} = -0.547 \end{Bmatrix}$	$\begin{Bmatrix} Intercept = 18.9 \\ E_T = 0.0024 \\ T = 1.08 \\ C_{H_2S} = -0.214 \end{Bmatrix}$	0.0015
	Neutralization Depth (mm)	N	$0.057C_{H_2S} + 0.05T + 0.004E_T - 0.6$	0.97		$\begin{Bmatrix} Intercept = -4.6 \\ E_T = 0.0027 \\ T = -0.13 \\ C_{H_2S} = 0.021 \end{Bmatrix}$	$\begin{Bmatrix} Intercept = 3.47 \\ E_T = 0.0063 \\ T = 0.229 \\ C_{H_2S} = 0.0942 \end{Bmatrix}$	0.0003

for all four physical parameters, indicating high predictive ability. The coefficient of determination in FA-GPm models lies between 0.74-0.96 representing reasonably high confidence level.

4. Conclusion

Durability of low-calcium fly ash based geopolymer mortar (FA-GPm) and sulphate resistant Portland cement mortar (SRPCm) was investigated under two testing environments i.e. natural sewer and 1.5 % sulphuric acid solution. Outcomes are as follows:

Overall, SRPCm experienced greater deterioration in terms of mass loss, dry bulk density, compressive strength and surface disintegration compared to FA-GPm. Indeed, FA-GPm specimens remained visually intact in both testing conditions. However, neutralization depth, corrosion depth and reduction in pH were identified to be greater in FA-GPm compared to SRPCm under both testing conditions. This was consistent with the greater increase in volume of permeable voids detected in FA-GPm specimens.

After 24 months of infield exposure, no thenardite mineral was observed with the microstructure of FA-GPm and matrix showed major development of meso-porosity beside a loss of alkalinity and dealumination of N-A-S-H gel matrix. This loss of aluminium resulted in the formation of highly porous siliceous gel matrix which is durable to further acid attack making it resilient towards MICC. Minor gypsum formation was also identified within the microstructure of FA-GPm after infield exposure, but gypsum precipitation was not widespread as observed in SRPCm due to the low calcium content of FA-GPm.

The widespread crystallization of gypsum within the corroded regions of SRPCm is responsible of the major micro-cracking, loss in strength, loss of mass and surface disintegration observed on SRPCm specimens.

Natural MICC investigations suggest that FA-GPm could perform better than SRPCm if used in plain concrete members or as a sacrificial coating material because of its resilience to surface disintegration. However, the much greater neutralization depth and reduction in pH observed in FA-GPm could be a concern for steel reinforced concrete members.

Regarding sulfuric acid testing, the assessment of the neutralization of the acid solution showed that FA-GPm has a greater capacity of acid consumption compared to SRPCm due to greater alkali leaching from the geopolymer matrix than calcium leaching from C-S-H matrix.

Mineral characterization using XRD and FTIR analysis showed almost similar reaction products as the ones observed in natural conditions in both FA-GPm and SRPCm. However, by comparing the mechanisms of deterioration observed in natural aggressive sewer environment to that observed after exposure to sulphuric acid solution, significant differences can be highlighted. For both mortar types, the mechanism of neutralization in natural sewer condition is governed by the simultaneous carbonation and H_2S acidification, beside the interaction with microorganisms which produces sulphuric acid and causes localized deteriorations within the microstructure after penetration. In sulphuric acid exposure, neutralization of mortar is due to the widespread diffusion of SO_4^{2-} and H^+ ions from the acid solution causing an alkalinity loss and generalized deteriorations. Hence, this testing method cannot be used to estimate the service life and to design the sewage infrastructure.

Lastly, based on data collected from 2 years field experimentation, empirical models are proposed with high coefficient of determination to estimate the performance of FA-GPm and SRPCm in terms of time-dependent depth of corrosion, surface pH, mass loss and neutralization

depth as a function of exposure time, temperature and H2S concentration.

Authorship conformation form

All authors have participated in (a) conception and design, or analysis and interpretation of the data; (b) drafting the article or revising it critically for important intellectual content; and (c) approval of the final version.

Data availability

The raw/processed data required to reproduce these findings cannot be shared at this time as the data also forms part of an ongoing study.

CRediT authorship contribution statement

Hammad A. Khan: Methodology, Investigation, Writing - original draft. **Arnaud Castel:** Conceptualization, Supervision. **Mohammad S.H. Khan:** Project administration, Writing - review & editing.

Declaration of Competing Interest

The authors have no affiliation with any organization with a direct or indirect financial interest in the subject matter discussed in the manuscript

Acknowledgements

This research is financed by Cooperative Research Centres (CRC) for Low Carbon Living (grant number RP1020), an Australian Government initiative. The assistance of laboratory staff in the structures laboratory of school of civil and environmental engineering and Mark Wainwright analytical centre at the University of New South Wales is acknowledged here. Authors would also like to acknowledge Sydney Water for providing access to North head waste water treatment plant in Manly, Sydney, Australia.

References

[1] M.G.D. Gutiérrez-Padilla, A. Bielefeldt, S. Ovtchinnikov, M. Hernandez, J. Silverstein, Biogenic sulfuric acid attack on different types of commercially produced concrete sewer pipes, Cem. Concr. Res. 40 (2010) 293–301.
[2] C. Grengg, F. Mittermayr, A. Baldermann, M.E. Böttcher, A. Leis, G. Koraimann, P. Grunert, M. Dietzel, Microbiologically induced concrete corrosion: a case study from a combined sewer network, Cem. Concr. Res. 77 (2015) 16–25.
[3] S. MortezaNia, F. Othman, Cost analysis of pipes for application in sewage systems, Material & Design 33 (2012) 356–361.
[4] H.S. Jensen, Hydrogen Sulfide Induced Concrete Corrosion of Sewer Networks, Aalborg University, 2009.
[5] N. De Belie, J. Monteny, A. Beeldens, E. Vincke, D. Van Gemert, W. Verstraete, Experimental research and prediction of the effect of chemical and biogenic sulfuric acid on different types of commercially produced concrete sewer pipes, Cem. Concr. Res. 34 (2004) 2223–2236.
[6] J. Monteny, E. Vincke, A. Beeldens, N. De Belie, L. Taerwe, D. Van Gemert, W. Verstraete, Chemical, Microbiological, and In Situ test Methods for Biogenic Sulfuric Acid Corrosion of Concrete, Cem. Concr. Res. 30 (2000) 623–634.
[7] P.C. Hewlett, M. Liska, Lea's Chemistry of Cement and Concrete, 5th ed., Edward Arnold Ltd., London, England, 2017.
[8] H.F.W. Taylor, Cement Chemistry, 2nd ed., (1997).
[9] W. Kurdowski, Cement and Concrete Chemistry, Springer, Dordrecht, 2014.
[10] R.L. Islander, J.S. Devinny, F. Mansfeld, A. Postyn, H. Shih, Microbial ecology of crown corrosion in sewers, journal of environmental engineering, ASCE 117 (1991) 751–770.
[11] A.P. Joseph, J. Keller, H. Bustamante, P.L. Bond, Surface neutralization and H_2S oxidation at early stages of sewer corrosion: influence of temperature, relative humidity and H_2S concentration, Water Res. 46 (2012) 4235–4245.
[12] E. Vincke, E. Van Wanseele, J. Monteny, A. Beeldens, N. De Belie, L. Taerwe, D. Van Gemert, V. W, Influence of polymer addition on biogenic sulfuric acid attack of concrete, Int. Biodeterior. Biodegradation 49 (2002) 283–292.
[13] C. Grengg, F. Mittermayr, N. Ukrainczyk, G. Koraimann, S. Kienesberger, M. Dietzel, Advances in concrete materials for sewer systems affected by microbial induced concrete corrosion: a review, Water Res. 134 (2018) 341–352.
[14] D.J. Roberts, D. Nica, G. Zuo, J.L. Davis, Quantifying microbially induced deterioration of concrete: initial studies, Int. Biodeterior. Biodegradation 49 (2002) 227–234.
[15] C. Parker, The corrosion of the concrete I. The isolation of a species of bacterium associated with the corrosion of concrete exposed to atmospheres containing hydrogen sulfide, Aust. J. Exp. Biol. Med. Sci. 23 (1945) 81–90.
[16] A. Bielefeldt, M.G.D. Gutierrez-Padilla, S. Ovtchinnikov, J. Silverstein, M. Hernandez, Bacterial kinetics of sulfur oxidizing Bacteria and their biodeterioration rates of concrete sewer pipe samples, J. Environ. Eng. 136 (2010) 731–738.
[17] M.W. House, W.J. Weiss, Review of microbially induced corrosion and comments on needs related to testing procedures, 4th International Conference on the Durability of Concrete Structures, Purdue University, West Lafayette, IN, USA, 2014, pp. 94–103.
[18] S. Okabe, M. Odagiri, T. Ito, H. Satoh, Succession of sulfur-oxidizing Bacteria in the microbial community on corroding concrete in sewer systems, Appl. Environ. Microbiol. 73 (2007) 971–980.
[19] J.L. Davis, D. Nica, K. Shields, D.J. Roberts, Analysis of concrete from corroded sewer pipe, Int. Biodeterior. Biodegradation 42 (1998) 75–84.
[20] T. Mori, T. Nonaka, K. Tazaki, M. Koga, Y. Hikosaka, S. Noda, Interactions of nutrients, moisture and pH on microbial corrosion of concrete sewer pipes, Water Res. 26 (1992) 29–37.
[21] J.F. Marquez-Peñaranda, M. Sanchez-Silva, J. Husserl, E. Bastidas-Arteaga, Effects of biodeterioration on the mechanical properties of concrete, Mater. Struct. 49 (2016) 4085–4099.
[22] F. Pacheco-Torgal, J. Castro-Gomes, S. Jalali, Alkali-activated binders: A review Part 1. Historical background, terminology, reaction mechanisms and hydration products, Constr. Build. Mater. 22 (2008) 1305–1314.
[23] J. Davidovits, Properties of geopolymer cements, in: first International Conference on Alkaline cements and concretes, Scientific Research Institute on Binders and Materials, KIEV State Technical University, KIEV, Ukraine, 1994, pp. 131–149.
[24] S.A. Bernal, J.L. Provis, V. Rose, R.Md. Gutiérrez, High-resolution X-ray diffraction and fluorescence microscopy characterization of alkali-activated slag-metakaolin binders, J. Am. Ceram. Soc. 96 (2013) 1951–1957.
[25] T. Bakharev, Resistance of geopolymer materials to acid attack, Cem. Concr. Res. 35 (2005) 658–670.
[26] J. Davidovits, Geopolymer Chemistry and Applications, Geopolymer Institute, 2008.
[27] A. Allahverdi, F. Škvára, Sulfuric acid attack on hardened paste of geopolymer cements part 1. Mechanism of corrosion at relatively high concentrations, Ceramics Silikaty 49 (2005) 225–229.
[28] M. Albitar, M.S. Mohamed Ali, P. Visintin, M. Drechsler, Durability evaluation of geopolymer and conventional concretes, Constr. Build. Mater. 136 (2017) 374–385.
[29] N.K. Lee, H.K. Lee, Influence of the slag content on the chloride and sulfuric acid resistances of alkali-activated fly ash/slag paste, Cem. Concr. Compos. 72 (2016) 168–179.
[30] R.R. Lloyd, J.L. Provis, J.S.J. van Deventer, Acid resistance of inorganic polymer binders. 1. Corrosion rate, Mater. Struct. 45 (2012) 1–14.
[31] M. Alexander, A. Bertron, N. De Belie, Performance of Cement-Based Materials in Aggressive Aqueous Environments, Springer, Ghent, 2013.
[32] N.I. Fattuhi, B.P. Hughes, The performance of cement paste and concrete subjected to sulphuric acid attack, Cem. Concr. Res. 18 (1988) 545–553.
[33] M.G.D. Gutierrez-Padilla, Activity of Sulfur Oxidizing Microorganisms and Impacts on Concrete Pipe Corrosion, University of Colorado, 2007.
[34] J. Herisson, E. Van Hullebusch, M. Moletta-Denat, P. Taquet, T. Chaussadent, Toward an accelerated biodeterioration test to understand the behavior of Portland and calcium aluminate cementitious materials in sewer networks, Int. Biodeterior. Biodegradation 84 (2013) 236–243.
[35] H.A. Khan, M.S.H. Khan, A. Castel, J. Sunarho, Deterioration of alkali-activated mortars exposed to natural aggressive sewer environment, Constr. Build. Mater. 186 (2018) 577–597.
[36] H.A. Khan, A. Castel, M.S.H. Khan, A.H. Mahmood, Durability of calcium aluminate and sulphate resistant Portland cement based mortars in aggressive sewer environment and sulphuric acid, Cem. Concr. Res. 124 (2019) 105852.
[37] D.K.B. Thistlethwayte, The Control of Sulphides in Sewerage Systems, Butterworths Pty Ltd, Sydney, Australia, 1972.
[38] T. Wells, R.E. Melchers, Modelling concrete deterioration in sewers using theory and field observations, Cem. Concr. Res. 77 (2015) 82–96.
[39] M.W. Kiliswa, Composition and Microstructure of Concrete Mixtures Subjected to Biogenic Acid Corrosion and Their Role in Corrosion Prediction of Concrete Outfall Sewers, University of Cape Town, 2016.
[40] M. Diercks, W. Sand, E. Bock, Microbial corrosion of concrete, Experientia 47 (1991) 514–516.
[41] J.M. Pluym-Berkhout, J. Mijnsbergen, R.B. Polder, Rioleringen (II), biogene zwavelzuuraantasting, Cement 9 (1989) 16–20.
[42] ASTM C642, Standard test method for density, absorption, and voids in hardened concrete, ASTM International, West Conshohocken, PA, 2013.
[43] C.D. Parker, Mechanics of corrosion of concrete sewers by hydrogen sulfide, Sewage Ind. Waste. 23 (1951) 1477–1485.
[44] C.D. Parker, The corrosion of concrete 2. The function of Thiobacillus concretivorus (NOV. SPEC.) in the corrosion of concrete exposed to atmospheres containing hydrogen sulphides, Aust. J. Exp. Biol. Med. Sci. 23 (1945) 91–98.
[45] T. Wells, R.E. Melchers, An observation-based model for corrosion of concrete sewers under aggressive conditions, Cem. Concr. Res. 61–62 (2014) 1–10.
[46] ASTM C109 / C109M, Standard test method for compressive strength of hydraulic

cement mortars (using 2-in. or [50-mm] cube specimens), ASTM International, West Conshohocken, PA, 2016.
[47] M.T. Bassuoni, N.L. Nehdi, Resistance of self-consolidating concrete to sulfuric acid attack with consecutive pH reduction, Cem. Concr. Res. 37 (2007) 1070–1084.
[48] F. Rendell, R. Jauberthie, The deterioration of mortar in sulphate environments, Constr. Build. Mater. 13 (1999) 321–327.
[49] X.J. Song, Durability of fly ash based geopolymer concrete against sulphuric acid attack, 10DBMC International Conference on Durability of Building Materials and Components, Lyon, France, 2005.
[50] S. Thokchom, P. Ghosh, S. Ghosh, Resistance of fly ash based geopolymer mortars in sulfuric acid, ARPN Journal of Engineering and Applied Sciences 4 (2009) 65–70.
[51] V. Räsänen, V. Penttala, The pH measurement of concrete and smoothing mortar using a concrete powder suspension, Cem. Concr. Res. 34 (2004) 813–820.
[52] E.K. Attiogbe, S.H. Rizkalla, Response of concrete to sulfuric acid attack, Aci Mater. J. 85 (1988) 481–488.
[53] R.E. Beddoe, H.W. Dorner, Modelling acid attack on concrete: part I. The essential mechanisms, Cem. Concr. Res. 35 (2005) 2333–2339.
[54] A. Bertron, J. Duchesne, G. Escadeillas, Accelerated tests of hardened cement pastes alteration by organic acids: analysis of the pH effect, Cem. Concr. Res. 35 (2005) 155–166.
[55] V. Pavlík, Corrosion of hardened cement paste by acetic and nitric acids part I: calculation of corrosion depth, Cem. Concr. Res. 24 (1994) 551–562.
[56] K.L. Scrivener, A.K. Crumbie, P. Laugesen, The interfacial transition zone (ITZ) between cement paste and aggregate in concrete, Interface Sci. 12 (2004) 411–421.
[57] T. Haile, G. Nakhla, E. Allouche, Evaluation of the resistance of mortars coated with silver bearing zeolite to bacterial-induced corrosion, Corros. Sci. 50 (2008) 713–720.
[58] J.P. Skalny, J. Marchand, I. Odler, Sulfate Attack on Concrete, Spon Press, London, 2002.
[59] J. Monteny, N. De Belie, E. Vinckeb, W. Verstraeteb, L. Taerwe, Chemical and microbiological tests to simulate sulfuric acid corrosion of polymer-modified concrete, Cem. Concr. Res. 31 (2001) 1359–1365.
[60] T.A. Aiken, J. Kwasny, W. Sha, M.N. Soutsos, Effect of slag content and activator dosage on the resistance of fly ash geopolymer binders to sulfuric acid attack, Cem. Concr. Res. 111 (2018) 23–40.
[61] P. Garcés, M.C. Andrade, A. Saez, M.C. Alonso, Corrosion of reinforcing steel in neutral and acid solutions simulating the electrolytic environments in the micropores of concrete in the propagation period, Corros. Sci. 47 (2005) 289–306.
[62] M.S.H. Khan, A. Castel, A. Noushini, Carbonation of a low-calcium fly ash geopolymer concrete, Mag. Concr. Res. 69 (2017) 24–34.
[63] S.K. Roy, K.B. Poh, D.O. Northwood, Durability of concrete-accelerated carbonation and weathering studies, Build. Environ. 34 (1999) 597–606.
[64] D.O. McPolin, P.A. Basheer, A.E. Long, K.T. Grattan, T. Sun, New test method to obtain pH profiles due to carbonation of concretes containing supplementary cementitious materials, J. Mater. Civ. Eng. 19 (2007) 936–946.
[65] D.O. McPolin, P.A. Basheer, A.E. Long, Carbonation and pH in mortars manufactured with supplementary cementitious materials, J. Mater. Civ. Eng. 21 (2009) 217–225.
[66] T.A. Aiken, W. Sha, J. Kwasny, M.N. Soutsos, Resistance of geopolymer and Portland cement based systems to silage effluent attack, Cem. Concr. Res. 92 (2017) 56–65.
[67] S.A. Bernal, J.L. Provis, B. Walkley, R. San Nicolas, J.D. Gehman, D.G. Brice, A.R. Kilcullen, P. Duxson, J.S.J. van Deventer, Gel nanostructure in alkali-activated binders based on slag and fly ash, and effects of accelerated carbonation, Cem. Concr. Res. 53 (2013) 127–144.
[68] J.L. Provis, R.J. Myers, C.E. White, V. Rose, J.S.J. van Deventer, X-ray microtomography shows pore structure and tortuosity in alkali-activated binders, Cem. Concr. Res. 42 (2012) 855–864.
[69] T. Bakharev, J.G. Sanjayan, Y.-B. Cheng, Resistance of alkali-activated slag concrete to carbonation, Cem. Concr. Res. 31 (2001) 1277–1283.
[70] M.A.M. Ariffin, M.A.R. Bhutta, M.W. Hussin, M.M. Tahir, N. Aziah, Sulfuric acid resistance of blended ash geopolymer concrete, Constr. Build. Mater. 43 (2013) 80–86.
[71] E. Gruyaert, P.V.D. Heede, M. Maes, N. De Belie, Investigation of the influence of blast-furnace slag on the resistance of concrete against organic acid or sulphate attack by means of accelerated degradation tests, Cem. Concr. Res. 42 (2012) 173–185.
[72] A. Allahverdi, F. Škvára, Nitric acid attack on hardened paste of geopolymeric cements, Ceram. - Silik. 45 (2001) 143–149.
[73] A.A. Ramezanianpour, A. Pilvar, M. Mahdikhani, F. Moodi, Practical evaluation of relationship between concrete resistivity, water penetration, rapid chloride penetration and compressive strength, Constr. Build. Mater. 25 (2011) 2472–2479.
[74] M.S.H. Khan, A. Castel, A. Akbarnezhada, S.J. Foster, M. Smith, Utilisation of steel furnace slag coarse aggregate in a low calcium fly ash geopolymer concrete, Cem. Concr. Res. 89 (2016) 220–229.
[75] E.I. Diaz, E.N. Allouche, S. Eklund, Factors affecting the suitability of fly ash As source material for geopolymers, Fuel 89 (2010) 992–996.
[76] A. Ferna´ndez-Jime´nez, A. Palomo, characterisation of fly ashes. Potential reactivity As alkaline cements, Fuel 82 (2003) 2259–2265.
[77] F. Puertas, S. Martínez-Ramírez, S. Alonso, T. Vázquez, Alkali-activated fly ash/slag cements: strength behaviour and hydration products, Cem. Concr. Res. 30 (2000) 1625–1632.
[78] F. Puertas, A. Fernández-Jiménez, Mineralogical and microstructural characterisation of alkali-activated fly ash/slag pastes, Cem. Concr. Compos. 25 (2003) 287–292.
[79] F. Puertas, M. Palacios, H. Manzano, J.S. Dolado, A. Rico, J. Rodríguez, A model for the C-A-S-H gel formed in alkali-activated slag cements, J. Eur. Ceram. Soc. 31 (2011) 2043–2056.
[80] W. De Muynck, N. De Belie, W. Verstraete, Effectiveness of admixtures, surface treatments and antimicrobial compounds against biogenic sulfuric acid corrosion of concrete, Cem. Concr. Compos. 31 (2009) 163–170.
[81] M. O'Connell, C. McNally, M.G. Richardson, Biochemical attack on concrete in wastewater applications: a state of the art review, Cem. Concr. Compos. 32 (2010) 479–485.
[82] Y. Lo, H.M. Lee, Curing effects on carbonation of concrete using a phenolphthalein indicator and Fourier-transform infrared spectroscopy, Build. Environ. 37 (2002) 507–514.
[83] A. Hajimohammadi, J.L. Provis, J.S.J. van Deventer, The effect of silica availability on the mechanism of geopolymerisation, Cem. Concr. Res. 41 (2011) 210–216.
[84] I. García-Lodeiro, A. Fernández-Jiménez, M.T. Blanco, A. Palomo, FTIR study of the sol–gel synthesis of cementitious gels: C–S–H and N–a–S–H, J. Solgel Sci. Technol. 45 (2008) 63–72.
[85] C. Shi, A.F. Jiménez, A. Palomo, New cements for the 21st century: the pursuit of an alternative to Portland cement, Cem. Concr. Res. 41 (2011) 750–763.
[86] M. Pérez, T. Vázquez, F. Triviño, Study of stabilized phases in high alumina cement mortars Part I Hydration at elevated temperatures followed by carbonation, Cem. Concr. Res. 13 (1983) 759–770.
[87] M. Torres-Carrasco, C. Rodríguez-Puertas, Md.M. Alonso, F. Puertas, Alkali activated slag cements using waste glass as alternative activators. Rheological behaviour, Boletãn La Soc. Espaã ± ola Cerã¡mica Y Vidr. 54 (2015) 45–57.
[88] M.M. Radwan, M. Heikal, H.H.M. Darweesh, Hydration characteristics and durability of calcium aluminate cement containing some blended systems, Silicates Industriels Belgian Ceramic Society 70 (2005) 41–50.
[89] L. Fernández-Carrasco, J. Rius, C. Miravitlles, Supercritical carbonation of calcium aluminate cement, Cem. Concr. Res. 38 (2008) 1033–1037.
[90] V.N. Nosov, N.G. Frolova, V.F. Kamyshov, IR spectra of calcium sulfate semihydrates, J. Appl. Spectrosc. 24 (1976) 509–511.
[91] S. Borhan, S. Hesaraki, S. Ahmadzadeh-Asl, Evaluation of colloidal silica suspension as efficient additive for improving physicochemical and in vitro biological properties of calcium sulfate-based nanocomposite bone cement, J. Mater. Sci. Mater. Med. 21 (2010) 3171–3181.
[92] H. Siad, M. Lachemi, M. Sahmaran, K.M.A. Hossain, Effect of glass powder on sulfuric acid resistance of cementitious materials, Constr. Build. Mater. 113 (2016) 163–173.
[93] C. Grengg, F. Mittermayr, G. Koraimann, F. Konrad, M. Szabó, A. Demeny, M. Dietzel, The decisive role of acidophilic bacteria in concrete sewer networks: a new model for fast progressing microbial concrete corrosion, Cem. Concr. Res. 101 (2017) 93–101.
[94] S.A. Bernal, E.D. Rodriguez, R.M. de Gutiérrez, J.L. Provis, Performance of alkali-activated slag mortars exposed to acids, J. Sustain. Cem. Mater. 1 (2012) 138–151.
[95] I. Ismail, S.A. Bernal, J.L. Provis, R.S. Nicolas, S. Hamdan, J.S.J. Van Deventer, Modification of phase evolution in alkali-activated blast furnace slag by the incorporation of fly ash, Cem. Concr. Compos. 45 (2014) 125–135.
[96] I. Garcia-Lodeiro, A. Palomo, A. Fernández-Jiménez, D.E. Macphee, Compatibility studies between N-A-S-H and C-A-S-H gels. Study in the ternary diagram Na2O–CaO–Al2O3–SiO2–H2O, Cem. Concr. Res. 41 (2011) 923–931.
[97] N.K. Lee, H.K. Lee, Reactivity and reaction products of alkali-activated, fly ash/slag paste, Constr. Build. Mater. 81 (2015) 303–312.
[98] A. Allahverdi, F. Škvára, Acidic corrosion of hydrated cement based materials - Part 2. Kinetics of the phenomenon and mathematical models, Ceramics Silikaty 44 (2000) 152–160.
[99] H. Yuan, P. Dangla, P. Chatellier, T. Chaussadent, Degradation modelling of concrete submitted to sulfuric acid attack, Cem. Concr. Res. 53 (2013) 267–277.
[100] H. Nielsen Asbjørn, T. Hvitved-Jacobsen, S. Jensen Henriette, J. Vollertsen, Experimental evaluation of the stoichiometry of sulfide-related concrete sewer corrosion, J. Environ. Eng. 140 (2014) 04013009.
[101] A. Bielefeldt, D. Gutierrez-Padilla Ma. Guadalupe, S. Ovtchinnikov, J. Silverstein, M. Hernandez, Bacterial kinetics of sulfur oxidizing Bacteria and their biodeterioration rates of concrete sewer pipe samples, J. Environ. Eng. 136 (2010) 731–738.
[102] G. Jiang, J. Keller, P.L. Bond, Determining the long-term effects of H2S concentration, relative humidity and air temperature on concrete sewer corrosion, Water Res. 65 (2014) 157–169.
[103] D. Wackerly, W. Mendenhall, R.L. Scheaffer, Mathematical Statistics With Applications, Thomson Higher Education, Belmont, CA, USA, 2008.